SPECIAL OWLeS COLLECTION

Identification of Convective Boundary Layer Depth over the Great Lakes Region Using Aircraft Observations: A Comparison of Various Methods

SUDHEER R. BHIMIREDDY[a] AND DAVID A. R. KRISTOVICH[a]

[a] *Climate and Atmospheric Science Section, Division of State Water Survey, Prairie Research Institute, University of Illinois Urbana–Champaign, Champaign, Illinois*

(Manuscript received 13 July 2023, in final form 11 January 2024, accepted 16 January 2024)

ABSTRACT: This study evaluates the methods of identifying the height z_i of the top of the convective boundary layer (CBL) during winter (December and January) over the Great Lakes and nearby land areas using observations taken by the University of Wyoming King Air research aircraft during the Lake-Induced Convection Experiment (1997/98) and Ontario Winter Lake-effect Systems (2013/14) field campaigns. Since CBLs facilitate vertical mixing near the surface, the most direct measurement of z_i is that above which the vertical velocity turbulent fluctuations are weak or absent. Thus, we use z_i from the turbulence method as the "reference value" to which z_i from other methods, based on bulk Richardson number (Ri_b), liquid water content, and vertical gradients of potential temperature, relative humidity, and water vapor mixing ratio, are compared. The potential temperature gradient method using a threshold value of 0.015 K m^{-1} for soundings over land and 0.011 K m^{-1} for soundings over lake provided the estimates of z_i that are most consistent with the turbulence method. The Ri_b threshold-based method, commonly used in numerical simulation studies, underestimated z_i. Analyzing the methods' performance on the averaging window z_{avg} we recommend using $z_{\mathrm{avg}} = 20$ or 50 m for z_i estimations for lake-effect boundary layers. The present dataset consists of both cloudy and cloud-free boundary layers, some having decoupled boundary layers above the inversion top. Because cases of decoupled boundary layers appear to be formed by nearby synoptic storms, we recommend use of the more general term, elevated mixed layers.

SIGNIFICANCE STATEMENT: The depth z_i of the convective atmospheric boundary layer (CBL) strongly influences precipitation rates during lake-effect snowstorms (LES). However, various z_i approximation methods produce significantly different results. This study utilizes extensive concurrently collected observations by project aircraft during two LES field studies [Lake-Induced Convection Experiment (Lake-ICE) and OWLeS] to assess how z_i from common estimation methods compare with "reference" z_i derived from turbulent fluctuations, a direct measure of CBL mixing. For soundings taken both over land and lake; with cloudy or cloud-free conditions, potential temperature gradient (PTG) methods provided the best agreement with the reference z_i. A method commonly employed in numerical simulations performed relatively poorly. Interestingly, the PTG method worked equally well for "coupled" and elevated decoupled CBLs, commonly associated with nearby cyclones.

KEYWORDS: Lake effects; Boundary layer; Mixed layer; Convective-scale processes; Aircraft observations; Soundings

1. Introduction

The atmospheric planetary boundary layer (PBL), the shallow layer through which Earth's surface initially influences the overlying atmosphere, is a fundamental feature directly or indirectly affecting most processes within the troposphere. However, the PBL, and the turbulent mixing processes within, evolve at size and time scales that are currently too small to explicitly simulate in mesoscale, regional, or global atmospheric numerical models. Therefore, PBL processes in such numerical models must be represented by bulk values (boundary layer depth, turbulent kinetic energy, etc.) approximated by parameterizations.

Scientific understanding has evolved for PBL that develop over quasi-uniform surfaces, particularly over land areas, to over highly nonuniform surface covers and topographic features where multiple local internal PBL can interact (LeMone et al. 2019). Among the current challenges and opportunities highlighted by LeMone et al. (2019) are understanding complex interchanges between boundary layers (BL) and low clouds, including the "interplay between microphysics,

Denotes content that is immediately available upon publication as open access.

Bhimireddy's current affiliation: Cooperative Institute for Research in Environmental Sciences, University of Colorado Boulder, Boulder, Colorado, and NOAA/Global Systems Laboratory, Boulder, Colorado.

Corresponding author: Sudheer R Bhimireddy, sudheer.r.bhimireddy@noaa.gov

DOI: 10.1175/JAMC-D-23-0114.1

turbulence, and dynamics involved in weakly to strongly coupled cloud-boundary layer systems." Understanding of such interactions requires, in part, the use of advanced observational systems capable of collecting data of turbulent fluctuations, state parameters and clouds, particularly at critical heights such as near the surface, at cloud base, and within the layer encompassing the PBL top.

Lake-effect (LE) PBLs include many of the processes at the cutting edge of PBL research, including additional complications due to the presence of both clouds and precipitation (Kristovich et al. 2019). LE storms can produce extremely hazardous weather and seasonal snowfall totals reaching three or more times that of surrounding regions (e.g., Braham and Dungey 1995). While much focus is on the considerable negative impacts on nearshore communities, lake-effect storms can also benefit some economic sectors (e.g., such as the winter recreation industry, Kristovich et al. 2017).

LE storms occur primarily in the fall and winter seasons (e.g., Rodriguez et al. 2007) when upwind cold air travels over relatively warm, unfrozen lakes. The result is a rapidly growing overlake convective PBL (CBL), driven by thermal heating near the surface energizing mixing throughout the layer and entrainment at the PBL top (e.g., Chang and Braham 1991). Additional energy is provided by latent heat processes associated with clouds in upper portions of the PBL and snow throughout its depth (Kristovich and Braham 1998), mesoscale circulations (e.g., Rodriguez et al. 2007; Laird and Kristovich 2004), and enhanced surface convergence and divergence near water–land boundaries (Kristovich et al. 2018). Evolution of the LE PBL structure with overlake fetch is very similar to the changes in daytime CBLs over land with time (e.g., Stull 1988; Lenschow 1973). As such, LE PBLs can be considered reasonable examples of convective PBL type, with added complexities associated with nonuniform surfaces and microphysical processes (e.g., Chang and Braham 1991; Zurn-Birkhimer et al. 2005).

A series of studies in the last few decades has led to a steady improvement in our understanding of LE PBLs. Recent field campaigns, such as Lake-Induced Convection Experiment (Lake-ICE; Kristovich et al. 2000) and Ontario Winter Lake-effect Systems (OWLeS; Kristovich et al. 2017) field effort conducted in 1997/98 and 2013/14, respectively, have augmented this understanding by providing valuable data. Several studies utilized data collected during these projects to examine mesoscale circulations (e.g., Bergmaier and Geerts 2020; Kosiba et al. 2019; Bergmaier et al. 2017; Cooper et al. 2000), evolution of the lake-effect system downwind from the lakes (e.g., Campbell and Steenburgh 2017; Welsh et al. 2016; Eipper et al. 2018, 2019; Veals et al. 2018; Campbell et al. 2016; Minder et al. 2015), and microphysical evolution (Steiger et al. 2018; Mulholland et al. 2017; Steenburgh and Campbell 2017; Barthold and Kristovich 2011). Additional studies examined the cross-lake evolution of the LE PBL (e.g., Schroeder et al. 2006; Zurn-Birkhimer et al. 2005; Kristovich et al. 2003; Young et al. 2000; Agee and Gilbert 1989). However, relatively few studies highlighted the three-dimensional spatiotemporal evolution of these boundary layers and how they relate to commonly observed CBLs in other environments (e.g., Kristovich et al. 2018; Agee and Hart 1990). The current study takes advantage of two field experiments focused on lake-effect storms, to assess the relative abilities of various methods of determining the depth of the CBL developed over other types of surfaces.

Past studies like Seibert et al. (2000), Seidel et al. (2010, 2012), Dai et al. (2011, 2014), Zhang et al. (2014), and Li et al. (2021) have tested and compared conventional (or operational) methods used to estimate the CBL depth based on observations taken from aircraft-borne sensors or radiosondes over a variety of land-cover areas. To the authors' knowledge, though, the applicability of various methods for determining the convective PBL depth over Great Lakes regions for LE conditions has not been tested.

The rest of the paper is structured as follows: section 2 details the dataset and analysis methods. Section 3 details the methodology followed to estimate the CBL depth based on various methods. Section 4 details the results of the CBL estimations for Lake-ICE and OWLeS campaigns and validity of CBL detection methods. Section 5 gives the summary of the results and implications for LE PBL–environmental condition relationships.

2. Data sources

The data used in this study were collected over and near Lake Michigan during Lake-ICE (Kristovich et al. 2000) and the Lake Ontario during OWLeS (Kristovich et al. 2017). Lake-ICE was conducted from 4 December 1997 to 22 January 1998; OWLeS was conducted between 12 December 2013 and 29 January 2014. During these campaigns, the University of Wyoming King Air (UWKA) research aircraft performed multiple flight patterns conducive to developing vertical soundings. During Lake-ICE, the NCAR Electra research aircraft also collected sounding data. We extracted sounding data for times when the UWKA altitude change was more than at least 1000 m while the horizontal distance covered was less than 20 km.

Figure 1 shows the locations of aircraft soundings during Lake-ICE and OWLeS. The 1000-m threshold was chosen so that the vertical structure of a significantly large depth of the atmosphere could be evaluated. As data from multiple aircraft during different campaigns was considered, the observations were initially averaged over 50-m vertical intervals (except for the turbulence measurements), which corresponds to 9–10 s in terms of time averaging as the average flight ascent rate was 5.3 m s^{-1}. This averaging also ensures that any variations in the observations due to sudden changes in the flight ascent rate would not cause unrepresentative vertical gradients.

Such aircraft-measured soundings provide a useful avenue for understanding PBL dynamics in complex LE conditions, including the magnitude of turbulent kinetic energy and the presence of clouds and precipitation. In situ observations taken during the aircraft flights are examined to compare the manner in which PBLs can be defined when such a wide variety of observed variables are available. Variables measured by research aircraft during the two projects are summarized in Kristovich et al. (2017) for OWLeS and Kristovich et al. (2000) for Lake-ICE. Variables that are derived from the aircraft observations for the present purpose of comparing the

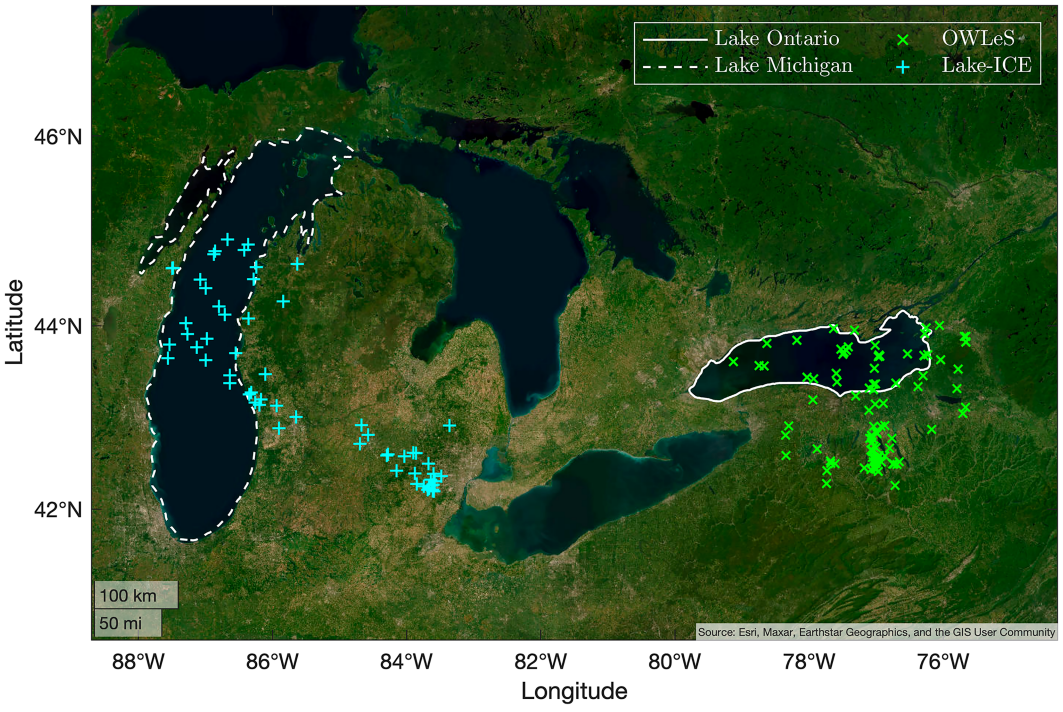

FIG. 1. Map of Lake Michigan (dashed line) and Lake Ontario (solid line) with aircraft soundings during Lake-ICE (plus signs) and OWLeS (times signs) campaigns considered in this study. Symbols indicate aircraft locations at the boundary layer depth identified by the turbulence method.

depth of the PBL are described in section 3 and are used in developing the sounding dataset for each field project.

During Lake-ICE (Kristovich et al. 2000), the UWKA research aircraft collected measurements at 20-Hz frequency while the NCAR Electra research aircraft collected measurements at 25-Hz frequency, which is sufficient to resolve turbulent fluctuations of thermodynamic and velocity fields (e.g., Young et al. 2000; Kristovich et al. 2003; Schroeder et al. 2006). During OWLeS (Kristovich et al. 2017), the UWKA research aircraft collected thermodynamic measurements at 25-Hz frequency, also sufficient to resolve turbulent fluctuations of thermodynamic and velocity fields.

3. CBL-top estimation and comparison methods

Methods employed in this study (except the turbulence method, with which all other methods are compared) either use a single variable measurement, for example relative humidity and liquid water content; or they use derived variables like mixing ratio, potential temperature, and Richardson number and so are subject to the uncertainty of the instruments used. In addition, the objective criteria used to determine the CBL top can be sensitive especially if it relies on a threshold value (discussed in detail in section 4b) that might not be applicable for data collected under different conditions with different instruments.

a. Turbulence method

The convection-driven mixed layer can be characterized by the presence of continuous turbulence. The height at which this continuous turbulence becomes weak and beyond which it ceases to exist could be treated as the CBL top (Stull 1988; Seibert et al. 2000). This standard definition of the CBL top gives rise to the turbulence method followed in this study. Using high-frequency observations from aircraft soundings, the turbulent fluctuations can be estimated. The CBL depth estimated by the turbulence method (TURB) is often treated as the "reference value" (Kaimal et al. 1982; Stull 1988).

Figure 2 shows an example of flight sounding data collected by the UWKA in a dry CBL during the OWLeS campaign. The subplot for the turbulent fluctuations of vertical velocity w' shows a clear distinction (horizontal line at 1550 m) between the CBL having strong turbulent fluctuations and the free atmosphere where the turbulence fluctuations were much smaller or absent. These fluctuations were obtained after any slow variations were removed using a high-pass filter of 0.1 Hz (corresponding to an average vertical displacement of 53 m for the average aircraft ascent rate of 5.3 m s^{-1}) as described by Chang and Braham (1991) and Wang et al. (1999). Similar profiles were examined (not shown) for other components of the velocity (u' and v'). The CBL depth is extracted by performing a continuous wavelet transform (Morlet wavelet) on the vertical velocity fluctuations and detecting the height beyond which the scale-averaged and normalized wavelet power spectra become less than 0.01 or 1% (Fig. 3).

b. Gradient methods

Gradient methods rely on the observations of scalars such as potential temperature $\overline{\theta}$, relative humidity (RH), and

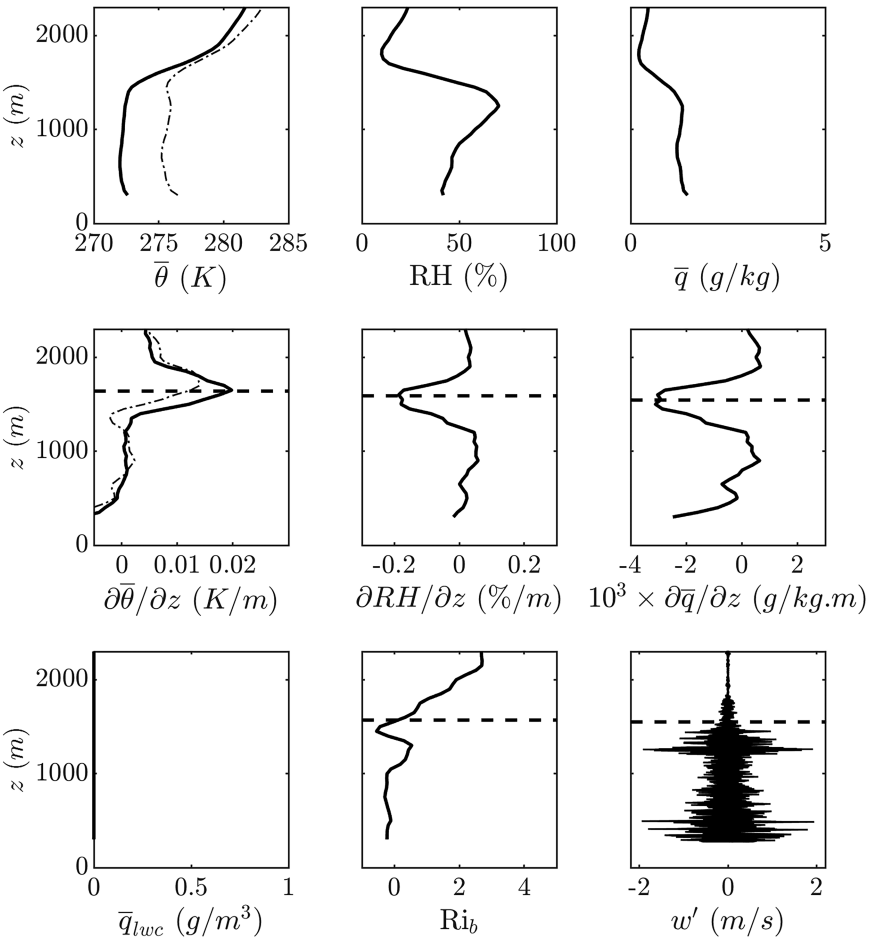

FIG. 2. UWKA observations of (top) (left) potential temperature, (center) relative humidity, (right) mixing ratio; (middle) gradients of (left) potential temperature, (center) mixing ratio, (right) relative humidity; and (bottom) (left) liquid water content, (center) bulk Richardson number, and (right) vertical velocity fluctuations during the 7 Dec 2013 flight sounding from 1634 to 1642 UTC (i.e., from 1134 to 1142 LT; LT = local time = UTC − 5 h) near Lake Ontario. The horizontal dashed line in each graph represents the boundary layer top identified by each respective method as the x-axis variable. The dash–dot line in the $\overline{\theta}$ and $\partial\overline{\theta}/\partial z$ subplots represent the respective quantities for equivalent potential temperature.

mixing ratio $\overline{q}$. One advantage of gradient methods is that the required inputs ($\overline{\theta}$ and RH) could be obtained from rawinsonde observations, which are less expensive and less complex than aircraft observations. Using potential temperature, the CBL depth is approximated as the height at which the potential temperature gradient $\partial\overline{\theta}/\partial z$ (PTG02) exceeds a certain threshold value (about 0.02 K m^{-1}; Santanello et al. 2005; Dai et al. 2011; LeMone et al. 2013). In other investigations, z_i is taken as the height where the potential temperature gradient is a maximum (PTGM; Hennemuth and Lammert 2006; Martucci et al. 2007). Both methods are tested in the present study. Similarly, using relative humidity and mixing ratio, the z_i value is often approximated as the height at which their respective gradients (∂RH/∂z and $\partial\overline{q}/\partial z$) [relative humidity gradient (RHG) and mixing ratio gradient (MRG)] were minimum (i.e., the height with the greatest magnitude of negative gradients) (Duncan et al. 2022). Gradient methods work well for most of the CBL types (Seidel et al. 2010, 2012) and are widely applicable because of their simplicity but PTG02 is sensitive to the choice of a threshold value. Figure 2 shows the profiles of mean RH, $\overline{\theta}$, $\overline{q}$, and their respective gradients. The $\partial\overline{\theta}/\partial z$ profile barely crossed the 0.02 K m^{-1} threshold at 1550 m. At the same height, the ∂RH/∂z and $\partial\overline{q}/\partial z$ profiles were observed to be minimum, making 1550 m the determined CBL depth based on the $\overline{\theta}$, RH, and $\overline{q}$. Later in the present study, we also test the sensitivity of the PTG02 method for various threshold values. In addition to the potential temperature, the equivalent potential temperature ($\overline{\theta}_e$) is also calculated (shown as dash–dot lines in Fig. 2). No significant differences are found between the CBL depth estimated using $\overline{\theta}_e$ and $\overline{\theta}$.

c. *Richardson number method*

Like gradient methods, the bulk Richardson number, or Ri$_b$, method (RIB) relies on the observations of mean wind

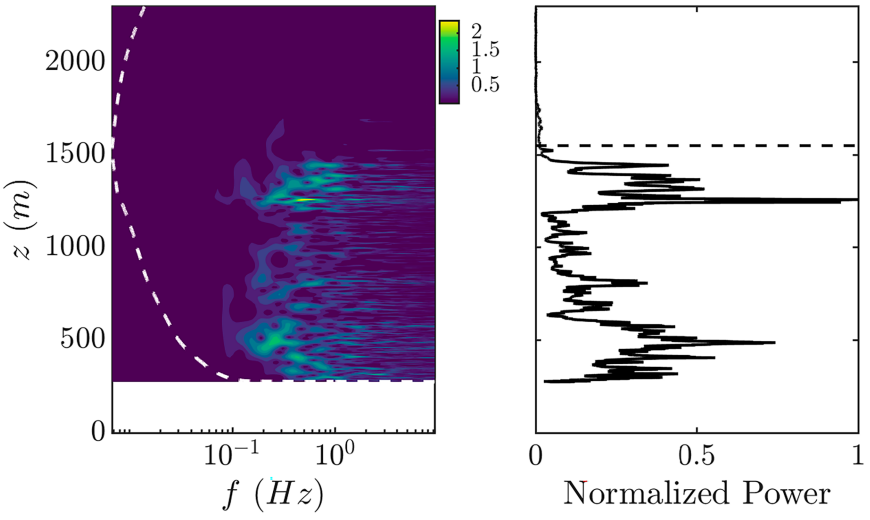

FIG. 3. (left) Wavelet power spectra magnitude and (right) scale-averaged and normalized wavelet power spectra for the vertical velocity fluctuations during the flight sounding shown in Fig. 2. The horizontal black dashed line in the right plot represents the boundary layer top.

velocity and mean potential temperature at different levels. The CBL top is defined when the Ri_b exceeds a critical value, often considered as 0.25 (Grimsdell and Angevine 1998; Zhang et al. 2011; Guo et al. 2021). Ri_b is defined as

$$\mathrm{Ri}_b = \frac{g\Delta z}{\overline{\theta}_v}\frac{\Delta\overline{\theta}_v}{\Delta\overline{u}^2 + \Delta\overline{v}^2},$$

where $\overline{\theta}_v$ is the mean virtual potential temperature calculated using the potential temperature and the mixing ratio, $\Delta\overline{\theta}_v$ is the change in virtual potential temperature across a layer of thickness Δz, and $\Delta\overline{u}$ and $\Delta\overline{v}$ are the changes in the streamwise and cross-stream wind speeds across the same layer. In the past, the RIB method worked well for climatological studies of the CBL top based on radiosonde observations over the continental United States (Seidel et al. 2012). However, the RIB method is sensitive to the threshold value of critical Richardson number. Many studies noted that a wide range of variations for the critical Richardson number between 0.25 and 0.5 were observed for CBLs (Garc et al. 2002; Zhang et al. 2014). In the numerical model parameterization schemes that uses Ri_b to define a CBL top, different values for critical Richardson number are being used; for example, a value of 0 is used in the Yonsei University scheme (Hong et al. 2006) and a value of 0.25 is used in the Asymmetric Convective Model, version 2, scheme (Pleim 2007). When the CBL is not well mixed and the shear within the CBL becomes too small, Ri_b becomes too large, and detecting the first level where Ri_b exceeds a critical value in such cases could result in a grossly underestimated z_i. To address this, we select the CBL top as the level beyond which the Ri_b exceeds the critical value consistently for 500 m (10 levels). Recently, Jozef et al. (2022) used similar method of detecting the CBL top using Ri_b only when it exceeded the critical value of 0.5 for 5 consecutive layers of the observations collected by a fixed wing unmanned aerial system during the Multidisciplinary Drifting Observatory for the Study of Arctic Climate (MOSAiC) campaign. The CBL top based on the Ri_b profile shown in Fig. 2 was estimated at 1570 m, as Ri_b consistently exceeds the threshold value of 0.25 beyond that height. This height is approximately 20 m above the CBL top estimated from turbulence and gradient methods in this sounding.

d. *Cloud-topped boundary layer method*

Studies of lake-effect snowstorms that incorporate cloud processes show that overwhelmingly, clouds should be considered a part of the upper CBL, which differentiates them from common overland CBLs (e.g., Chang and Braham 1991; Kristovich et al. 2003). Therefore, criteria using the cloud top are used here as another method to determine the top of the LE CBL. For the cloud-topped CBLs, Lenschow et al. (2000) recommended a threshold value of 0.04 g m^{-3} for the liquid water concentration (LWC) measured by the Forward Scattering Spectrometer Probe (FSSP) on board the NCAR Electra during the Dynamics and Chemistry of the Marine Stratocumulus (DYCOMS) experiment in July–August 1985. Lenschow et al. (2000) used this value to identify the cloud–clear-air interface and examined marine stratocumulus cloud decks. The value of 0.04 g m^{-3} was suggested to overcome instrument noise. For the present dataset, we identified a FSSP LWC value of 0.08 g m^{-3} as the lower limit to filter out the instrument noise and any baseline shift during both OWLeS and Lake-ICE field campaigns by looking at the LWC values in cloud-free flight legs. This value is higher than Lenschow et al. (2000) possibly because of the presence of snow particles in many of the soundings. The current dataset consists of both cloud-free (dry) and cloudy soundings. Figure 4 shows an example of flight sounding data collected by the UWKA in a cloud-topped CBL during the OWLeS campaign with liquid water detected between 1000- and 2000-m height. Similar to the CBL depth identified in dry sounding shown in Fig. 2, the CBL depth identified by respective methods are marked by black

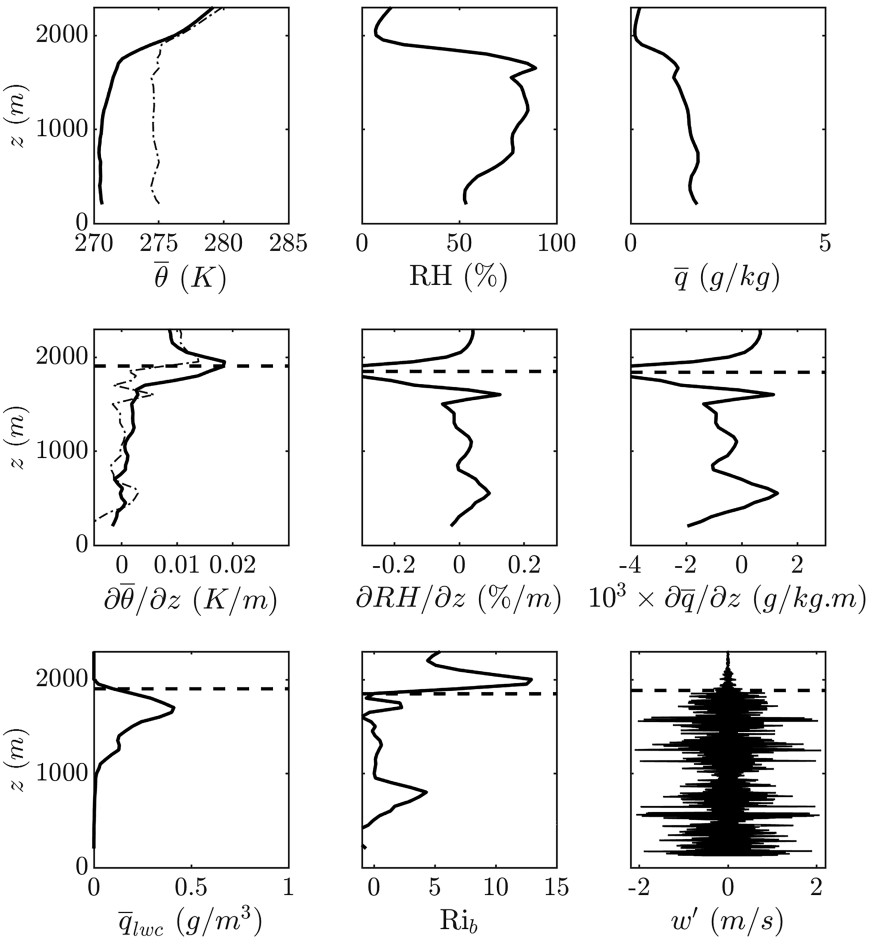

FIG. 4. As in Fig. 2, but during the 7 Dec 2013 flight sounding from 1700 to 1710 UTC (i.e., from 1200 to 1210 LT) over Lake Ontario.

dashed line in corresponding subplots of Fig. 4. Table 1 summarizes the methods used in this study and relevant literature.

e. Metrics for comparing z_i determination methods

The following metrics, named below, were used to compare the performance of CBL depth detection methods:

$$\text{IOA} = 1 - \frac{\sum_{i=1}^{n}(z_i - z_{i\text{turb}})^2}{\sum_{i=1}^{n}(|z_i - \overline{z}_{i\text{turb}}| + |z_{i\text{turb}} - \overline{z}_{i\text{turb}}|)^2},$$

$$\text{MBE} = \frac{\sum_{i=1}^{n}(z_i - z_{i\text{turb}})}{n},$$

$$\text{MAE} = \frac{\sum_{i=1}^{n}|z_i - z_{i\text{turb}}|}{n}, \quad \text{and}$$

$$c\text{RMSE} = \sqrt{\frac{\sum_{i=1}^{n}[(z_i - \overline{z}_i) - (z_{i\text{turb}} - \overline{z}_{i\text{turb}})]^2}{n}},$$

where z_i represents the CBL depth estimated by respective method, $z_{i\text{turb}}$ represents the CBL depth estimated by the turbulence method, n represents the number of flight soundings, and $\overline{z}_i$ and $\overline{z}_{i\text{turb}}$ represent the respective means. A method that would show good agreement with the TURB method would have an index of agreement (IOA) close to unity and mean absolute error (MAE), mean bias error (MBE), and centered RMSE (cRMSE) close to zero. The cRMSE is obtained after removing the bias from the error and so represents the random component of the error, whereas the MBE represents the systematic component of the error. In addition, the Pearson correlation coefficient R was also calculated. Because some of the soundings were performed over lake bodies, the datasets are divided into over land and lake to understand the influence of surface cover.

4. Results

a. Overview of boundary layers during Lake-ICE and OWLeS

Using the CBL depth determined by the turbulence method, the average CBL depth when it could be determined was

TABLE 1. Methods for estimating the CBL top. A total of 167 flight soundings were considered in the study. The value given in the parentheses represents the number of flight soundings through cloud-topped boundary layers. Note that Lenschow et al. (2000) used 0.04 g m^{-3} as the LWC threshold based on the observations from their study.

Variable	Method	Description	No. of flight soundings for which a potential BL top was identifiable	Relevant literature
w	TURB	Height at which the scale-averaged and normalized wavelet power spectra of the vertical velocity fluctuations become less than 1%	121 (58)	Stull (1988), Garratt (1994)
θ	PTGM	Height of max vertical gradient of θ	167 (78)	Hennemuth and Lammert (2006), Martucci et al. (2007)
θ	PTG02	Height at which vertical gradient of θ is higher than 0.02 K m^{-1}	94 (48)	Santanello et al. (2005)
RH	RHG	Height of min vertical gradient of RH	167 (78)	Garratt (1994), Seidel et al. (2010)
q	MRG	Height of min vertical gradient of q	167 (78)	Ao et al. (2008), Wang and Wang (2014)
Ri_b	RIB	Height at which the value becomes larger than 0.25	123 (57)	Vogelezang and Holtslag (1996), Seidel et al. (2010)
lwc	LWC	Height at which the value becomes smaller than 0.08 g m^{-3}	78	Lenschow et al. (2000)

1440 m during Lake-ICE and 1600 m during OWLeS. During Lake-ICE and OWLeS, the boundary layer grew deeper (not shown) near the downwind shores of the lakes, which might be expected due to the cumulative influence of over-lake convective motions driven by the relatively warm lake surface and surface convergence near the downwind shore. This matches the trend observed in the lake-effect literature (e.g., Kristovich et al. 2003; Schroeder et al. 2006; Barthold and Kristovich 2011). The average wind direction measured by aircraft within the boundary layer during Lake-ICE was 295° (aligned almost perpendicular to the long axis of Lake Michigan) and OWLeS was 269° (aligned parallel to the long axis of Lake Ontario). Because of the dominant westerly winds, soundings east of Lake Michigan, Lake Ontario and Lake Erie are subjected to the lake influence. Moreover, the shoreline and downwind regions of Lake Ontario could be influence by the lake-effect boundary layer generated due to the upwind Lake Erie and result in a deeper lake-effect boundary layer with increased turbulence magnitude as discussed in Kristovich et al. (2018). The range of mixed layer potential temperature within the boundary layer during Lake-ICE was from 258 to 284 K and during OWLeS was from 255 to 280 K over the lake. The PBL tended to be filled with liquid water cloud in the top half and snow filled throughout.

Based on their thermodynamic structure the aircraft soundings from the present dataset can be divided into two categories, namely, coupled (Figs. 2 and 4) and apparently decoupled boundary layers (Greybush et al. 2018). Coupled PBL represents the "classic" lake-effect structure with a well-mixed layer, topped by stable conditions (Figs. 2 and 4). As discussed later in section 5, the decoupled boundary layers exhibit an elevated mixed layer and are capped by an elevated secondary inversion aloft. While decoupled mixed layers have been studied for stratocumulus-topped or marine boundary layers (Jones et al. 2011; Dong et al. 2014; Nowak et al. 2021), rather few cases are discussed in the LE PBL literature. These decoupled boundary layers were observed in the aircraft-measured soundings during 5 of 11 days and 6 of 22 days for the duration of the Lake-ICE and OWLeS campaigns, respectively. The observed decoupled boundary layers are discussed in more detail in the discussion section.

b. Comparison of BL detection methods

A total of 167 flight soundings were considered in this study. Of these, 78 had clouds present, allowing for use of the cloud z_i-determination method. The performance metrics for all the methods for over land and over lake are given in Table 2. Figure 5 gives a detailed comparison of methods tested. In Fig. 5, we present the results when the aircraft passed through clouds separately from the dry (cloud free) cases to show the relative performance of methods in the presence of clouds. In addition, soundings over land and lake are also distinguished. With some scatter, the performance of methods for soundings through clouds was similar to each

TABLE 2. Performance metrics for various CBL detection criteria (see Table 1) calculated against the CBL depth estimated from turbulence method and divided into over land and lake.

Method		IOA	MBE	cRMSE	R
PTGM	Land	0.74	287	498	0.63
	Lake	0.78	277	562	0.71
PTG02	Land	0.78	96	451	0.61
	Lake	0.87	92	380	0.78
RHG	Land	0.72	288	557	0.61
	Lake	0.76	106	552	0.57
MRG	Land	0.76	31	584	0.63
	Lake	0.60	−147	637	0.35
RIB	Land	0.78	−247	432	0.69
	Lake	0.68	−409	413	0.62
LWC	Land	0.83	−13	416	0.70
	Lake	0.85	−138	340	0.74

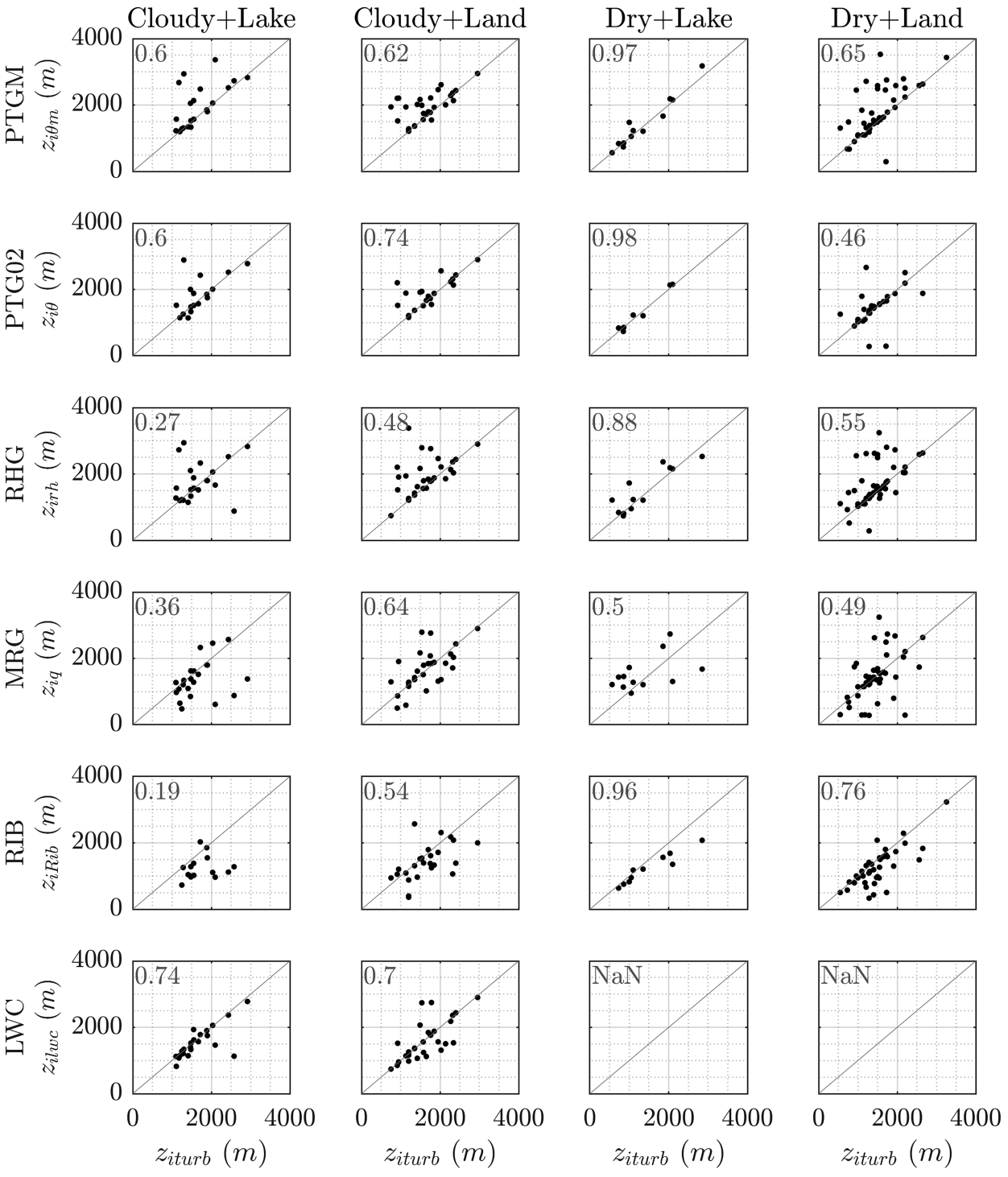

FIG. 5. Scatterplot of CBL depths estimated using, from top to bottom, maximum potential temperature gradient, potential temperature gradient, relative humidity gradient, mixing ratio gradient, critical Richardson number, and liquid water content methods compared with those from turbulence method during OWLeS and Lake-ICE campaigns. Each column corresponds to the cloudy or dry and land-cover conditions as given in the title of the first-row plots. Numbers given in the top-left corner of each plot represent the correlation coefficient.

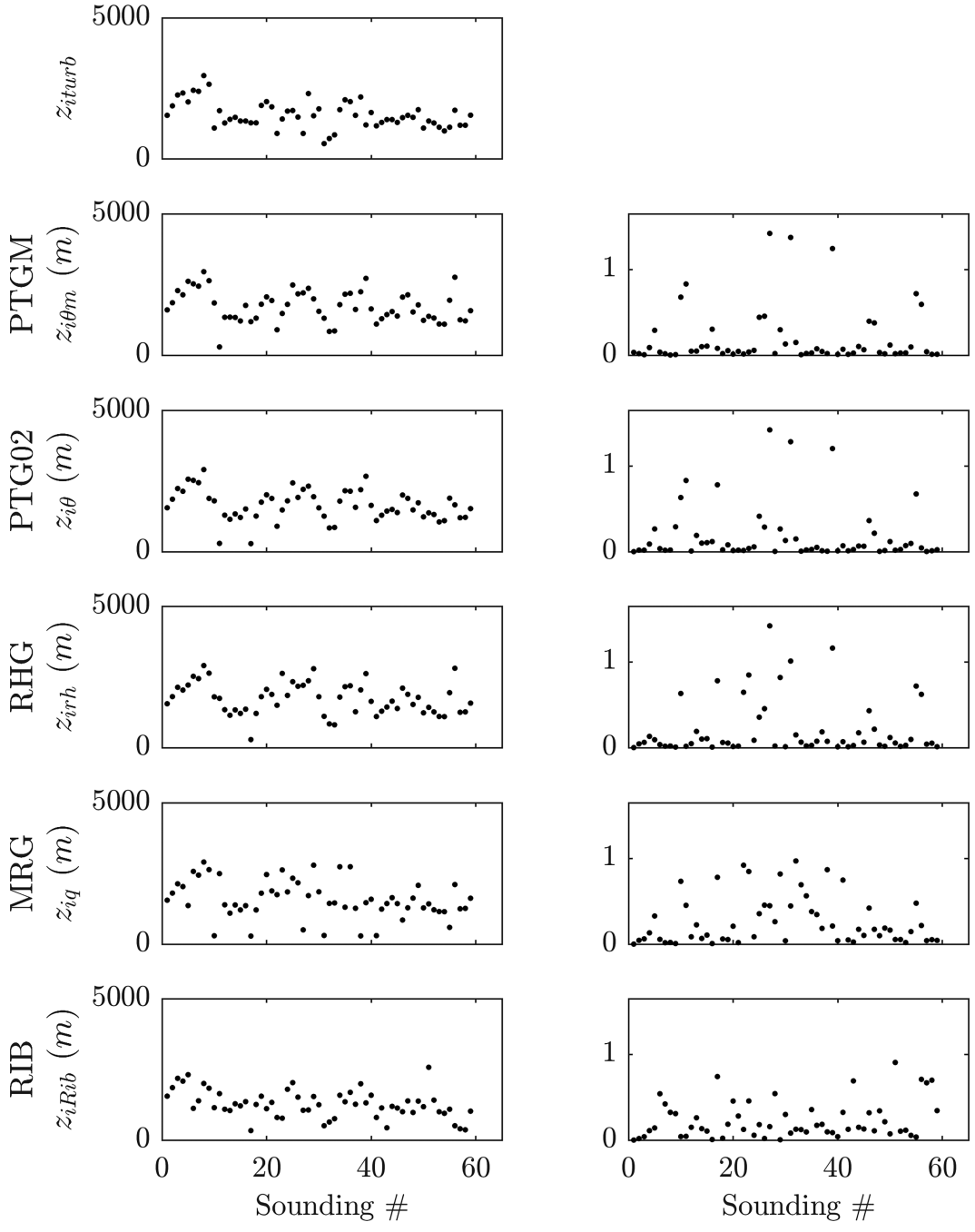

FIG. 6. (left) CBL depths estimated by TURB, PTGM, PTG02, RHG, MRG, and RIB methods during all OWLeS and Lake-ICE flight soundings. (right) Absolute relative error (i.e., $|z_i - z_{i\text{turb}}|/z_{i\text{turb}}$) for the datapoints in the left column. Data points for which the CBL depth is nonretrievable from either of the methods mentioned above were excluded from the plot.

other irrespective of land or lake cover underneath the sounding. Figure 5 also presents the individual correlation coefficient between the methods and the TURB method. Separating the data into cloudy/dry and land/lake categories reduced the number of data points in each category. This could impact the performance metrics, as seen from the "Dry+Lake" cases in Fig. 5, where the correlation coefficients are quite high ($\geq$0.88) except for the MRG method. When clouds are present in the sounding legs, the performance of methods (except for LWC) is seen to improve over land relative to over lake. Contrary to this, during dry soundings, the performance of methods is reduced over land relative to over lake. To verify

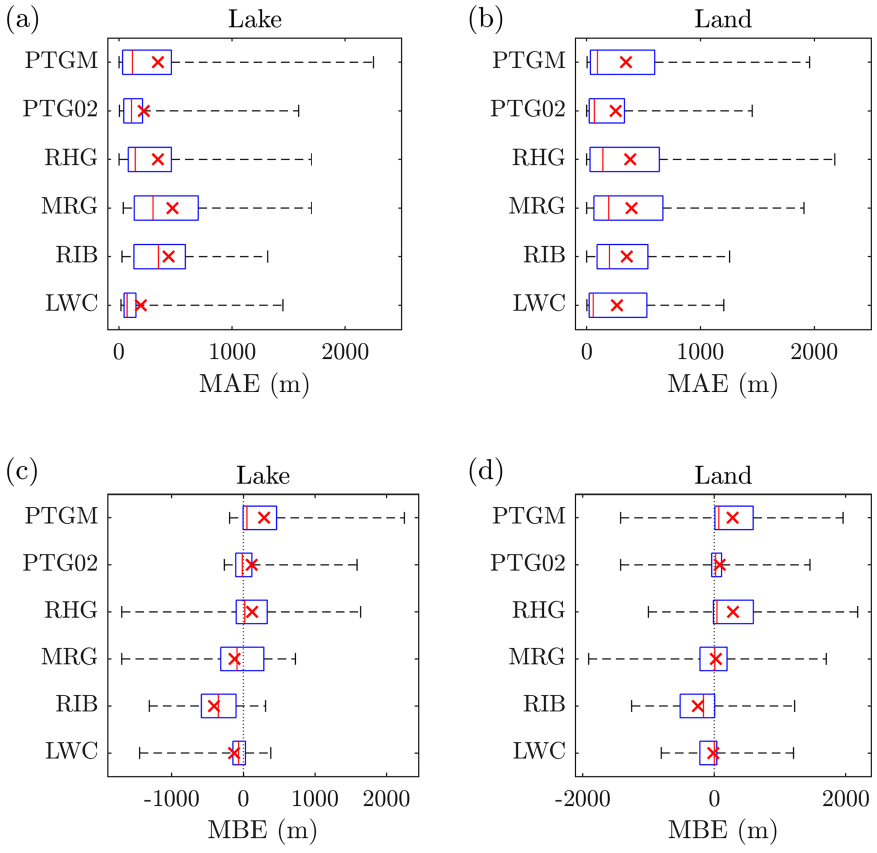

FIG. 7. Boxplot of (a),(b) mean absolute error and (c),(d) mean bias error for CBL depths estimated using different methods, as listed on the vertical axis, over (left) land and (right) lake. The vertical red line represents the median, the red cross represents the mean value, the box contains the interquartile range, and the whiskers extend to the minimum and maximum values.

whether the differences in z_i detected are distributed throughout the dataset, we show the soundings (about 59 in number) where a boundary layer depth was identified using all the methods tested in this study as well as the absolute error of the soundings in Fig. 6. The relative error for the RIB and MRG methods was consistently higher in comparison with other methods. The PTGM, PTG02, and RHG methods resulted in similar absolute errors.

Visual inspection of Fig. 5, and higher correlation coefficient values from Table 2 suggests that the spread of z_i against $z_{i\text{turb}}$ was small for PTGM and PTG methods as compared with other methods. Of all of the methods, the RIB method underestimated the CBL depth consistently. To illustrate the range of errors from the methods, we performed boxplot analysis (Fig. 7). To know the maximum errors, the boxplot analysis ignored outlier detection criteria. The mean and the median of the MAEs calculated for the PTG02 method were lowest in comparison with other methods for observations over land and lake (Figs. 7a,b). The mean and median of MAEs from the PTGM method were second lowest in comparison with other methods. While PTG02 and PTGM methods performed superior with low MAE values, their mean MBE values indicate a different behavior. From Figs. 7c and 7d, the PTGM method resulted in overestimation of CBL depth over land and lake. Based on the mean MBE values over lake, the MRG, RIB, and LWC methods underestimated the CBL depth; while over land, only the RIB method underestimated the CBL depth. Also, relative to the magnitude of MBE, the cRMSE values are greater (Table 2), meaning the random component of the error is greater than the systematic one independent of land cover.

The z_i estimated by the PTG02 method was close to the value given by TURB method with an IOA of 0.78 over land and 0.87 over lake, and an R value of 0.61 over land and 0.78 over lake. Except for the MBE and cRMSE over land, other metrics calculated for the PTG02 method were the best values among the methods used for cloud-free soundings. MBE depends on the means of the estimated and true values, so it is possible to have a 0 value MBE by relative errors cancelling each other (Chang and Hanna 2004). For observations taken over lake, the MRG method performed poorly with an IOA of 0.60, an R value of 0.35, and the cRMSE value of 637 m. For observations taken over land, the RHG method performed poorly with an IOA of 0.72, an R value of 0.61, and a cRMSE value of 557 m.

We tested the sensitivity of these methods on the lake versus land cover by combining the observations over lake and

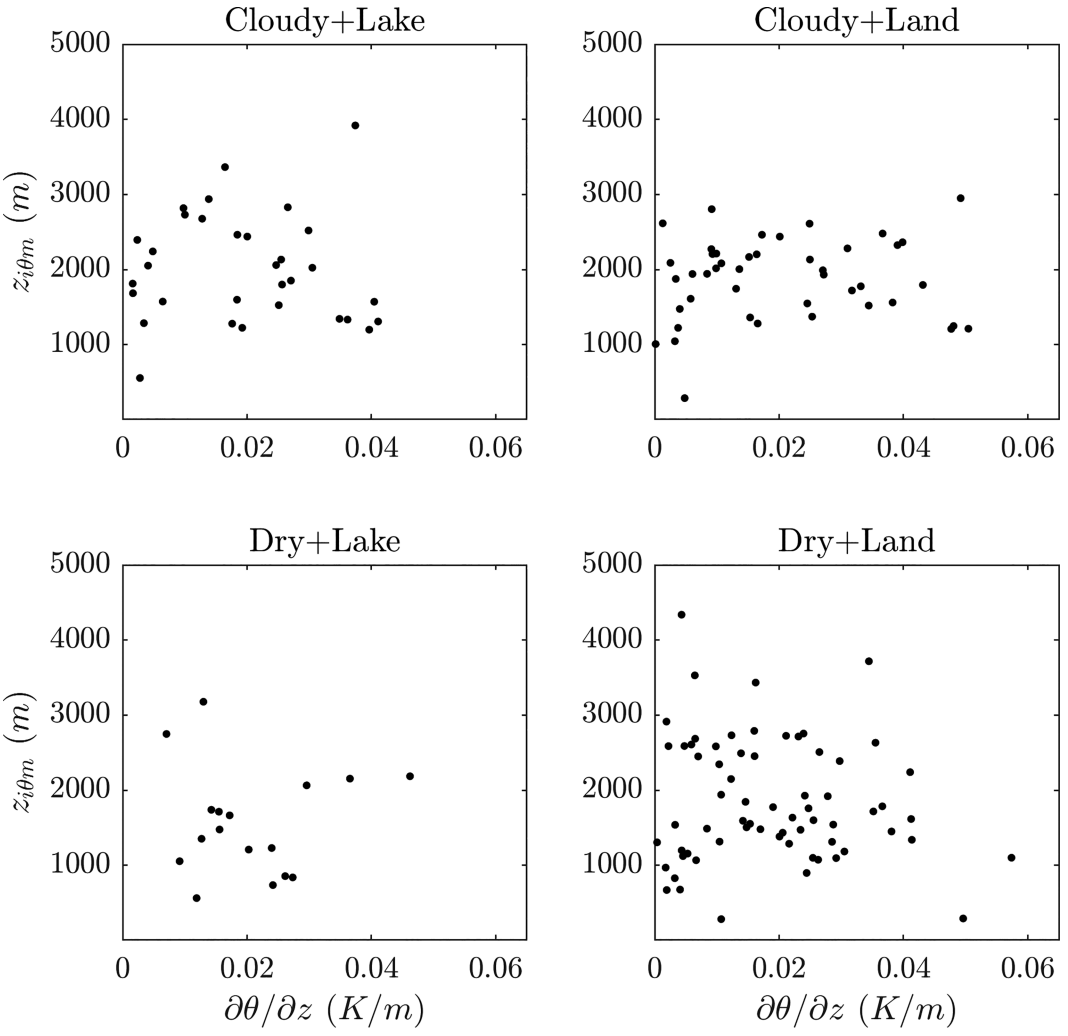

FIG. 8. Maximum potential temperature gradient magnitude at the corresponding boundary layer depth estimated using the PTGM method.

land and found that the PTG02 method performed superior to other methods.

The results from Table 2 indicate that the applicability of CBL detection methods using potential temperature is independent of the surface cover for LE PBLs. Figure 8 illustrates another sensitivity factor in our study: the choice of the $\partial\theta/\partial z$ threshold value. In the past, several studies have used different threshold values for estimating the CBL depth based on their datasets, for example, Bianco and Wilczak (2002) used a value of 0.0083 K m^{-1} for CBL observations over land, while Zeng et al. (2004) used a value of 0.003 K m^{-1} for CBL observations over ocean. On the other hand, a maximum value of PTG was used in the past by Hennemuth and Lammert (2006) while detecting CBL depth over land and ocean, and Martucci et al. (2007) for observations over land. Dai et al. (2014) found that for clear weather and scattered fair-weather cumuli conditions, using a constant value of PTG in the range of 0.001–0.018 K m^{-1} (land) and 0.006–0.008 K m^{-1} (ocean) gave best results, while the maximum PTG approach worked well for stratocumulus-topped boundary layer. Figure 8 gives the magnitude of maximum PTG value and respective boundary layer depth identified by PTGM method in the current dataset. The maximum PTG value in the present study varied from 0.001 to 0.058 K m^{-1}. For cloud-free soundings over land, the MAE value for PTG method was estimated to be about 270 m (for a mean CBL depth of 1400 m). That translates to a relative error of 0.19, which is comparable to the relative error of 0.14 reported by Dai et al. (2014).

We performed sensitivity analysis by varying the threshold value for the PTG02 method in the range 0.001–0.06 K m^{-1} with 0.001 K m^{-1} increments and calculated the IOA performance metric. The PTG02 threshold value with the maximum IOA is listed in Table 3. Using PTG02 method, for soundings over land and lake, the highest IOA values of 0.85 and 0.94 were obtained for a PTG threshold value of 0.015 and 0.11 K m^{-1}, respectively (50 m averaging window). Similar to the PTG method, the RIB method also relies on a threshold value, the critical Richardson number. We performed

TABLE 3. Maximum IOA and potential temperature gradient value used to achieve maximum IOA for various datasets.

CBL over	Max IOA	PTG threshold ($K\ m^{-1}$)	Averaging window (m)
Land	0.82	0.019	20
Lake	0.93	0.019	
Land	0.85	0.015	50
Lake	0.94	0.011	
Land	0.86	0.013	100
Lake	0.96	0.007	

TABLE 4. Maximum IOA and critical Richardson number value used to achieve maximum IOA for various datasets.

CBL over	Max IOA	Critical Ri_b	Averaging window (m)
Land	0.82	0.80	20
Lake	0.93	1.45	
Land	0.86	0.65	50
Lake	0.95	1.6	
Land	0.95	0.55	100
Lake	0.84	2.0	

sensitivity analysis by varying the critical Ri_b value in the range 0.1–2 in 0.05 increments and calculated IOA as above and presented the results in Table 4. Our results gave a best critical Ri_b value of 0.65 for soundings over land, and 1.6 for soundings over lake. Dai et al. (2014), using BOREAS experiment dataset, varied critical Ri_b value in the range 0.25–3 and found RIB method performed poorly with very low detection score for the critical Ri_b range tested and concluded that RIB method is not recommended for application to the boundary layer depth detection during convective conditions.

c. *Effect of vertical resolution*

Aircraft soundings are useful and provide detailed observations of the atmosphere but are expensive to perform. On the other hand, balloon soundings are less expensive and can provide observations required to use some of the methods (other than turbulence and liquid water content methods). In addition to the balloon soundings, measurements of atmospheric backscatter or winds can also provide boundary layer top estimations (Kotthaus et al. 2023; Sagrestano 2023; Duncan et al. 2022). We tested the performance of the methods listed for 5-, 20-, 50-, 100-, 200-, and 300-m vertical averaging windows. This wide range of vertical averaging window was chosen to mimic vertical profile data provided by most of the balloon-borne instruments.

Figure 9 gives the variation of IOA, and R with vertical averaging window z_{avg} for different methods with soundings over land and lake. For the PTGM and RHG methods, the IOA, and R values remained nearly constant for different z_{avg}. Of all of the methods tested, PTG02 method was most sensitive to the z_{avg} value. For z_{avg} higher than 100 m, the PTG02 method performance decreased more rapidly over lake than land as IOA decreased. Interestingly, for observations over lake, before the performance of the PTG02 method decreased rapidly for $z_{avg} > 100$ m, it increased and performed best for $z_{avg} = 20$ m. However, for observations over land, no significant improvements were observed at $z_{avg} = 20$ m. Similar to the PTG02 methods performance over lake, the MRG method's performance is sensitive to z_{avg} value. MRG methods IOA over lake reduced as z_{avg} value increased from 5 to 100 m, and later increased modestly as the averaging window became coarser. RIB methods IOA over lake reduced overall as z_{avg} value increased. LWC methods IOA increased with increase in z_{avg} value up to 100 m and decreased slightly for z_{avg} values 200 and 300 m. This suggests a possible difference between the cloud-top level and the level where turbulent motions cease to exist; further analysis is required to investigate. Over land, all the methods except PTG02 performed approximately independent of vertical resolution. Over lake, only the PTGM method performed independent of vertical resolution. Based on IOAs, for soundings over lake, optimum z_{avg} value for different methods is 20 m for the PTGM, PTG02, and MRG methods and 100 m for the RHG and LWC methods. The difference in IOAs for 20 and 50 m for PTGM, PTG02, and MRG methods was less than 0.07. As lake-effect systems are often cloudy (especially over the lake); we recommend using $z_{avg} = 20$ or 50 m for boundary layer depth estimations.

We now calculate each method's efficiency (η) in detecting the boundary layer depth. η is similar to the detection rate used in Dai et al. (2014). It estimates the number of times the relative error ($\%\varepsilon = |z_i - z_{i\text{turb}}|/z_{i\text{turb}} \times 100$) from a method was less than a given value. As one would expect, η increases as the allowable $\%\varepsilon$ value is increased. Using the variation of η with $\%\varepsilon$, we can learn about when each method would result in a satisfactory performance. To investigate the dependence of η on relative error, we varied $\%\varepsilon$ from 5% to 100%. Relative error relaxes the allowed error depending on the boundary layer depth. For example, a 10% relative error for a 500 m deep boundary layer would mean the allowable error is ±50 m, while the same relative error for a 2000-m-deep boundary layer would make the allowable error to be ±200 m. Figure 10 gives the variation of η with $\%\varepsilon$. The η values varied most among the methods for a given $\%\varepsilon < 40\%$ and over lake soundings, while over the land this variation is much smaller. For $\%\varepsilon < 40\%$, the overall behavior of the methods remained the same, that is, PTG02 method performed best over land and lake while RIB method performed poorly over land, and MRG method performed poorly over lake. For a 5% relative error, PTG02 method had approximately 50% efficiency over land for all resolutions tested, while its performance varied with resolution over lake. The RIB method had 50% efficiency for all resolutions over land and lake when the relative error was in the range of 20%–25%. Even for 100% relative error, some methods had an efficiency less than 100%, suggesting that the boundary layer depth estimated by such methods differs from the true value by a significant amount. Such cases were identifiable from Fig. 6, for example, cases in between sounding 25 and 40 in Fig. 6 had shallow boundary layer depth below 1000 m while the boundary layer depth estimated by other methods (except MRG method) was more than 2000 m. Selecting a $\%\varepsilon$ that is acceptable depends on the specific

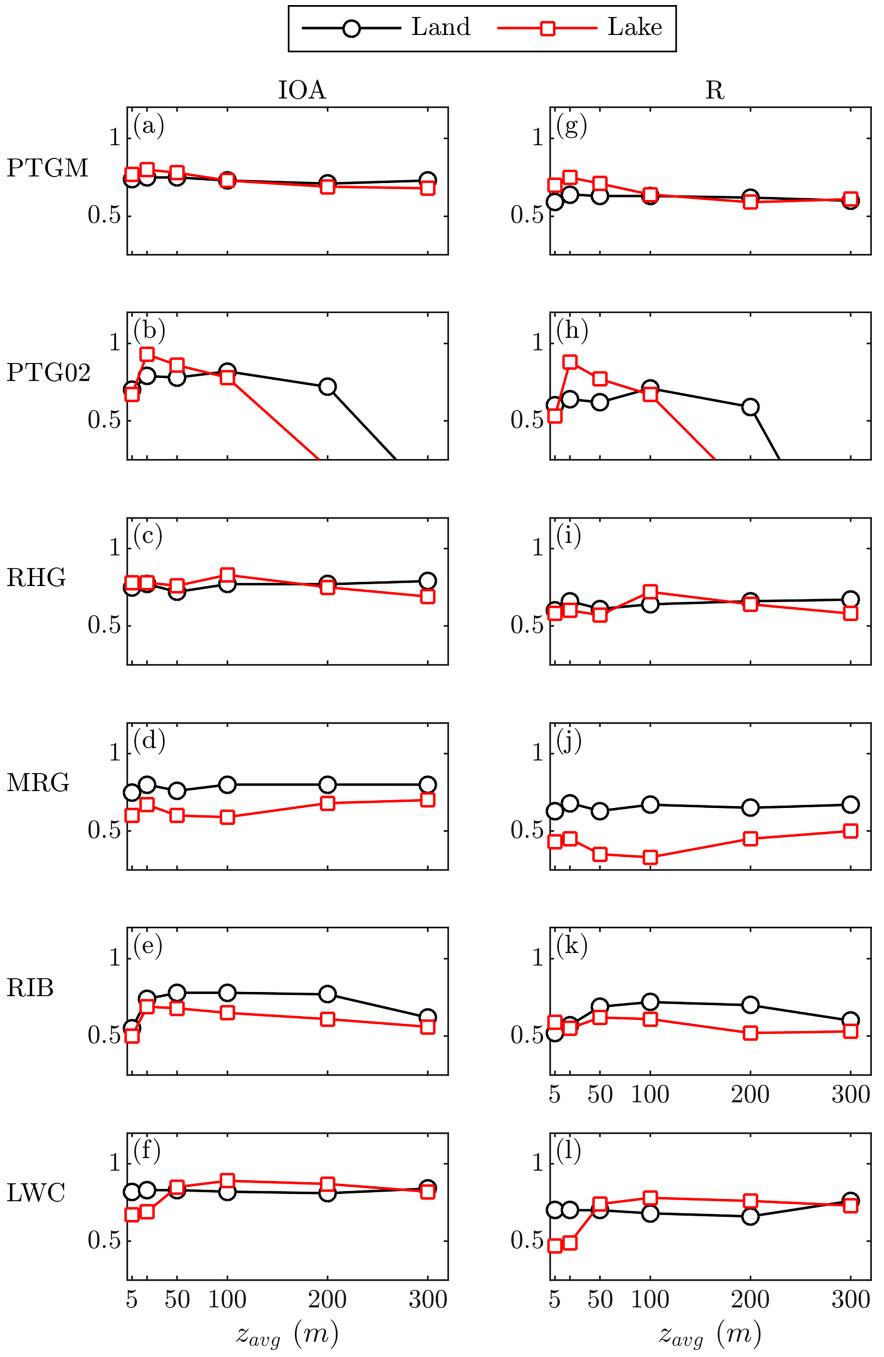

FIG. 9. Performance metrics (a)–(f) IOA and (g)–(l) R of methods for different vertical averaging windows. Each row corresponds to the method labeled on its left.

application for which z_i is to be detected. In case of CBLs that are just developing with weak convective motions but are capped by a well-defined inversion, the z_i is often shallow (<500 m) and even a 10%–20% (±100 m) error could be acceptable. Likewise, in CBLs that are developed and well mixed and have strong convective motions, the z_i is often in range of 2000–2500 m, meaning a 10%–20% error would be too large. As the lake-effect boundary layers grow along the lake (Chang and Braham 1991; Kristovich et al. 2018), a $\%\varepsilon$ that is acceptable for z_i detection at the upwind shore of the lake might result in large uncertainty at the downwind shore.

Overall, the effect of vertical resolution seems more sensitive to the methods' performance over lake than land. For a 50%, 25%, or 10% relative error, most of the methods tested respectively detected the true boundary layer depth at least 75%–80%, 50%–70%, or 10%–60% of the time.

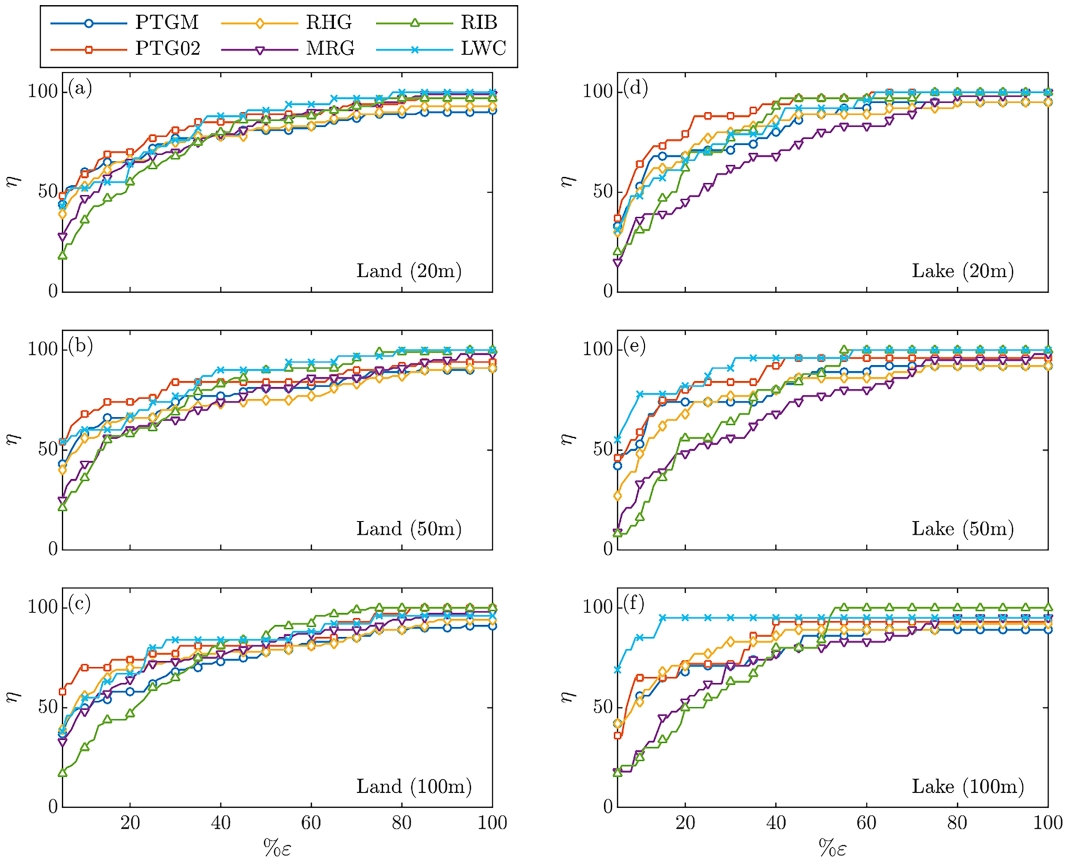

FIG. 10. Efficiency η of methods as a function of relative error ($\%\varepsilon$) for soundings over (a)–(c) land and (d)–(f) lake.

d. *Possible reasons for large differences between z_i detected by differing methods*

For this study, the z_i detected based on different variables resulted in very large differences when compared with the z_i detected from the TURB method. In this section, we go over the possible reasons for when the methods deviate. Overall, the cases with largest differences in estimated z_i, the CBL is much different than the "classic" case with well-developed mixed layer capped by an inversion. First, we discuss the situation where the reference z_i is not well defined. Although, TURB method is considered as the most reliable in estimating the CBL depth by recognizing the CBL with strong turbulent motions, it has been observed to be sensitive to the presence of clouds and/or wind shear (Wang et al. 1999; Moeng et al. 2005; Wang and Wang 2004). The present dataset also includes soundings where the TURB method failed to identify the CBL top due to the presence of strong vertical velocity fluctuations throughout the sounding levels (an example sounding is shown in section 5; Fig. 13). Of course, when the reference z_i is not well defined, comparisons between methods must be taken with caution.

Another situation where the z_i detected by methods differ by a considerable amount is when the CBL is not well mixed and/or has multiple cloud layers. An example is given in Fig. 11, where the z_i detected by the PTGM method matches closely with the TURB method, while the other methods greatly underestimated the z_i value. Moreover, the z_i from the minimum gradient methods (RHG and MRG) was the lowest and was detected just below the cloud base at 1000 m as seen from the LWC profile in Fig. 11. Even the bulk Richardson number exceeded the critical value around this height but not consistently for 500 m above that height. Therefore, the RIB method detected the base of the secondary cloud layer as z_i. In this case, the estimated z_i fell into three categories, the TURB and PTGM methods z_i (approximately 2700 m), the LWC and RIB methods (about 1400 m), and the MRG and RHG methods (near 1000 m). Such differences have been previously reported, such as cases where the maximum gradient of potential temperature might not always coincide with the cloud top (Lenschow et al. 2000; Wang and Wang 2014).

One way to improve the TURB method when it fails to identify the CBL depth for boundary layers having strong turbulent fluctuations in the vertical velocity, is to use the information from other methods or to test for the existence of elevated mixed layer(s). For example, looking at the vertical velocity turbulent fluctuations in Fig. 11, we can subjectively define four different layers, the first layer having strongest turbulent fluctuations up to 1100-m depth, capped by a layer of weak turbulent fluctuations extending up to 1900 m, a third layer with strong turbulent fluctuations between 1900 and 2800 m, and a fourth layer with near-zero turbulent fluctuations. The elevated turbulent layer corresponds to the cloud

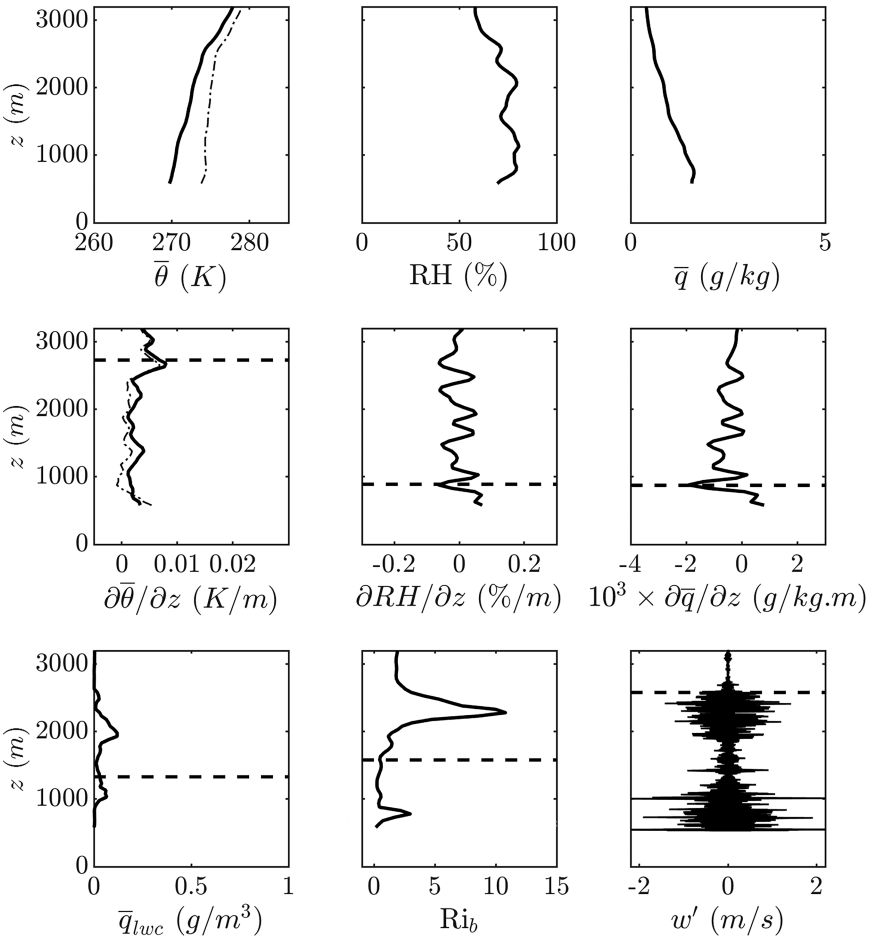

FIG. 11. As in Fig. 2, but during 11 Dec 2013 flight sounding from 1830 to 1837 UTC (i.e., from 1330 to 1337 LT) over Lake Ontario.

layer in which the liquid water content reached its maximum value around $z = 2000$ m. Likewise, the maximum or minimum gradient based methods performance could also be varied by either restricting the z_i detectable based on a maximum allowable CBL depth value (D. Zhang et al. 2022; J. Zhang et al. 2022) or by setting thresholds for the gradient based methods and number of sounding levels that reached that threshold values (Chen et al. 2023). Seidel et al. (2010) considered 4000 m above ground level as the upper limit to detect the z_i, so that the methods can avoid detecting any tropospheric features as z_i. Using the radiosonde observations collected over China from 2012 to 2020, J. Zhang et al. (2022) compared the z_i detected by the RIB, PTGM, MRG, and RHG methods and found that their performance is sensitive to the selection of a z_{max} value, that is, the maximum depth below which z_i tends to exist most of the time. Defining a z_{max} value for the present study is challenging, because the lake-effect CBL depth can change drastically from day to day and/or along the downwind of the lakes and/or can be subjected to the influence of upwind lakes (Chang and Braham 1991; Kristovich et al. 2018). While the cases described in this section are relatively infrequent, the variation in estimated z_i, is itself an indication of how well the CBL and higher altitude air characteristics match the classic case of a well-mixed layer topped by a strong inversion.

5. Discussion

As mentioned in section 1, several studies compared the CBL depth detection methods and gave recommendations on what method to use and a suitable threshold value if one exists. Dai et al. (2011) used aircraft and radiosonde observations taken during Surface Heat Budget of the Arctic Ocean (SHEBA) campaign to study the variation of boundary layer depth over the Arctic Ocean. With the mean CBL potential temperatures often below 273 K, SHEBA thermodynamic profiles are similar to LE profiles. For the sea ice surfaces in high latitudes, Dai et al. (2011) calculated the optimum threshold value of $\partial\theta/\partial z$ as 0.01 K m^{-1} when using potential temperature gradient method. In the present study, for soundings over lake, we estimated the optimum threshold value of $\partial\theta/\partial z$ as 0.019–0.007 K m^{-1} (20–100-m averaging), which is close to the Dai et al. (2011) value. However, the lake surface was not covered by ice.

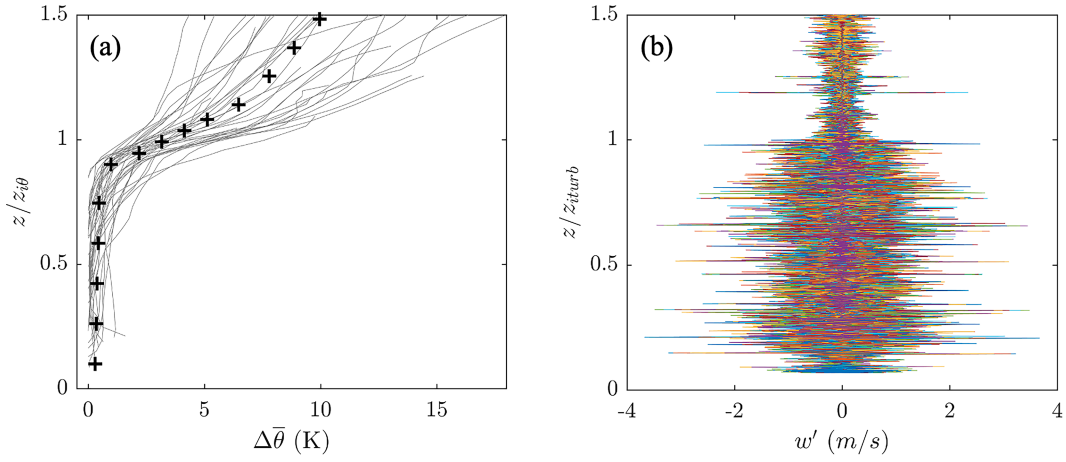

FIG. 12. Profiles of coupled LE PBL (a) potential temperature and (b) vertical velocity fluctuations during the OWLeS campaign. The height is normalized by the CBL depth estimated by respective variables, and $\Delta\overline{\theta} = \overline{\theta} - \min(\overline{\theta})$. The plus signs in (a) represent the average profile.

The structure of the CBL has a direct impact on the depth to which convective eddies can reach, the mass of dry air entrained across the boundary layer top, the growth rate of the boundary layer, the amount of latent heat released in the formation of clouds and, therefore, the efficacy of methods of determining their depth. In the case of LE storms, knowing the structure of LE PBL is important as its depth (or the related height of the "capping inversion"), in addition to other microphysical processes, dictates the snowfall rate received by the LE storms effected regions (e.g., Niziol et al. 1995; Kristovich et al. 2003). One of the unique aspects of LE boundary layers is the presence of clouds deep inside the boundary layer and sometimes above the boundary layer, in which case, seeding of snow particles into the existing boundary layer could occur (Schroeder et al. 2006).

An example of the coupled boundary layer is given in Fig. 2. Figure 12 shows the profiles of potential temperature difference [calculated as $\Delta\overline{\theta} = \overline{\theta} - \min(\overline{\theta})$ for each sounding] and vertical velocity fluctuations for all the soundings during OWLeS that exhibit a coupled boundary layer. The heights in Figs. 12a and 12b were normalized by the CBL depth estimated by the PTG02 and TURB methods, respectively. As seen from Fig. 12a, the $\overline{\theta}$ jump across the entrainment layer varied between 2 and 10 K suggesting a wide range of stability at the inversion. Such entrainment layers effectively slow the growth of the CBL and are thus often referred in the lake-effect snow forecasting literature to "capping inversions" that limit the lake-effect snowfall rate (e.g., Niziol et al. 1995; Niziol 1987). Figure 12b shows the turbulent fluctuations from the 25-Hz vertical velocity data during the soundings plotted in Fig. 12a. Above $z/z_{i\text{turb}} = 1$, w' magnitude reduced or became minimum when compared with the continuous turbulence present below.

Past studies have identified the existence of elevated decoupled layers based on the thermodynamic profiles of stratocumulus-topped marine boundary layers (Bretherton and Wyant 1997; Wood and Bretherton 2004; Jones et al. 2011; Dong et al. 2014; Ghate et al. 2015; Nowak et al. 2021). In these studies, the decoupling was observed to occur when the stratocumulus-topped boundary layers are advected over warm waters and the convective eddies cease to mix the contents up to the cloud base, resulting in the formation of a stable layer separating the stratocumulus layer that is no longer fed by the moisture supply from the well-mixed layer connected to the surface (Bretherton and Wyant 1997). Recently, Su et al. (2022) extended the decoupled layer classification developed for stratocumulus-topped boundary layer to cloud-topped boundary layer over land using the observations from U.S. Department of Energy's Atmospheric Radiation Measurement Southern Great Plains site. Su et al. (2022) considered an elevated layer to be decoupled if the cloud base is above the capping inversion of the CBL below. All of these studies relied on the information about the cloud (e.g., cloud-base height or cloud-base temperature) to determine if it exists in a coupled or a decoupled layer. Since LE clouds are primarily within the CBL, their methods would not be appropriate for identifying LE CBL decoupled layers.

Unlike Greybush et al. (2018), who found that elevated mixed layers were likely due to advection from lake-effect boundary layers advected from upwind lakes or upper-level outflow from lake-effect convective systems, we propose an alternate manner in which some of the decoupled boundary layers observed in the present study may have formed: the presence of a nearby synoptic storm system. An example decoupled mixed layer during OWLeS, observed on 1249 UTC 12 January 2014, is given in Fig. 13. Unlike a coupled BL with free atmosphere aloft, the potential temperature sounding in Fig. 13 shows an elevated mixed layer capped by a secondary inversion. Interestingly, this sounding shows the turbulent motions in the elevated mixed layer are much stronger than the CBL below. Figure 13 also indicates the presence of two distinct cloud layers, one near 1500 m and one near the top of the elevated mixed layer (about 2500 m). As seen in Fig. 14, such higher cloud decks can be associated with synoptic-scale disturbances that develop or move over/near the Great Lakes

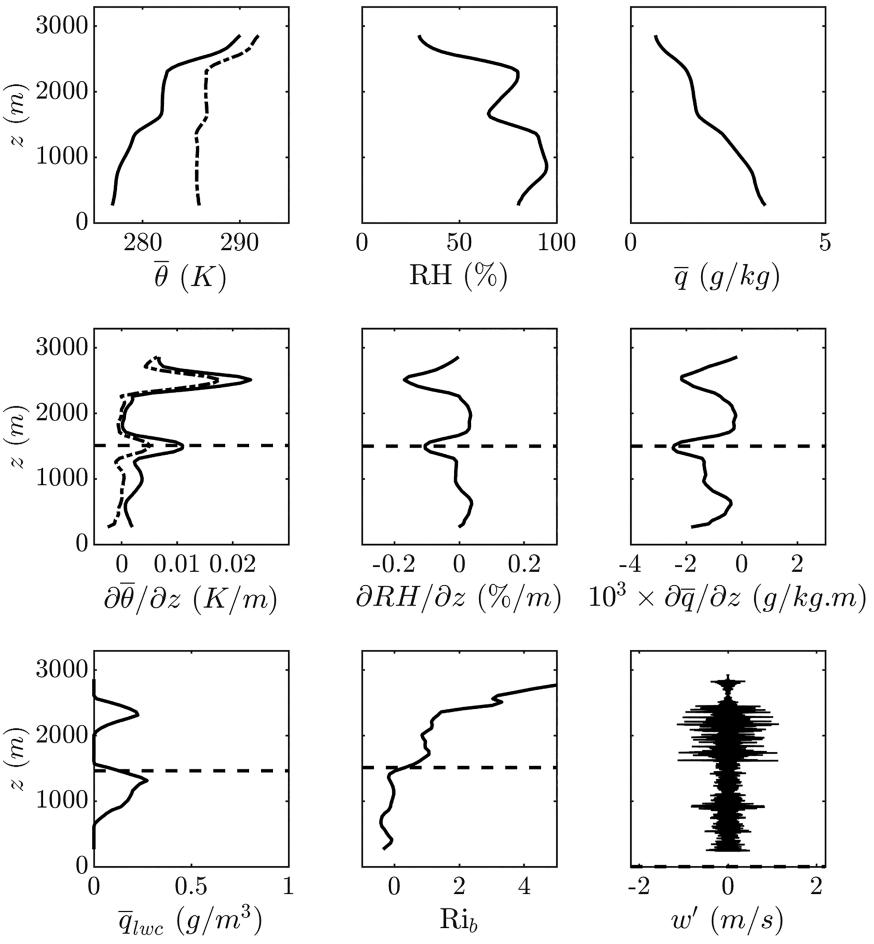

FIG. 13. As in Fig. 2, but during 12 Jan 2014 flight sounding from 1249 to 1257 UTC (i.e., from 0749 to 0757 LT) over Lake Ontario.

region. Preliminary analyses indicate that such elevated cloud layers can produce snow that can fall into the surface-based CBL and increase snowfall rates through the "seeder–feeder" process (e.g., Schroeder et al. 2006).

While Fig. 12 shows that coupled LE CBLs in OWLeS were quite similar, features of the elevated mixed layer cases varied considerably between cases. Figure 15 shows multiple soundings that are identified having an elevated mixed layer during OWLeS. The layer above the first inversion at $z_i/z_{i\theta} = 1$ is not always well mixed. However, a secondary inversion is present in the range $1.5 < z_i/z_{i\theta} < 2$. Such variations make it very difficult to make conclusive statements on the ideal identification methods. However, some studies (Schroeder et al. 2006; Chang and Braham 1991) have shown influences of elevated mixed layers (EMLs) on lake-effect processes.

Figure 16 gives a regional view of elevated mixed layer distributions based on NOAA/FAA soundings taken at as close a time as possible to two aircraft soundings. The top image reflects EML conditions near the time of the sounding shown in Fig. 13. The flight sounding EML is in an area extending from southwest of Lake Michigan and becomes shallower near a ridge in the mid–Great Lakes area and then deepens again over and near Lake Ontario. The relationship with synoptic features is intriguing and may suggest that synoptic systems, such as the warm front and associated cloud features (Fig. 14), play an important role in some EML cases. The local deepening of the EML within the larger-scale cloud field near Lake Ontario may indicate a lesser role of upwind Lake Erie and Lake Ontario influences on the soundings. Figure 16 shows two areas of deeper EMLs, east of Lake Ontario and extending west to over the northern plains. Based on synoptic analyses before and after this aircraft sounding time, these EML features are along a cold front that was moving southward across the Great Lakes with patches of low pressure along them. The regions of deeper EMLs were strongly correlated with frontal and cyclone center positions shown in the Daily Weather Map series at the next analysis time (1200 UTC 20 January 2014, not shown).

The presence of elevated mixed layers, especially when clouds and snow are present, could result in increased turbulent energy in the elevated mixed layer (such as seen in Fig. 13). While a full analysis of such cases is beyond the scope of this study, we note that for all such cases observed in this study, elevated clouds and EMLs apparently associated with

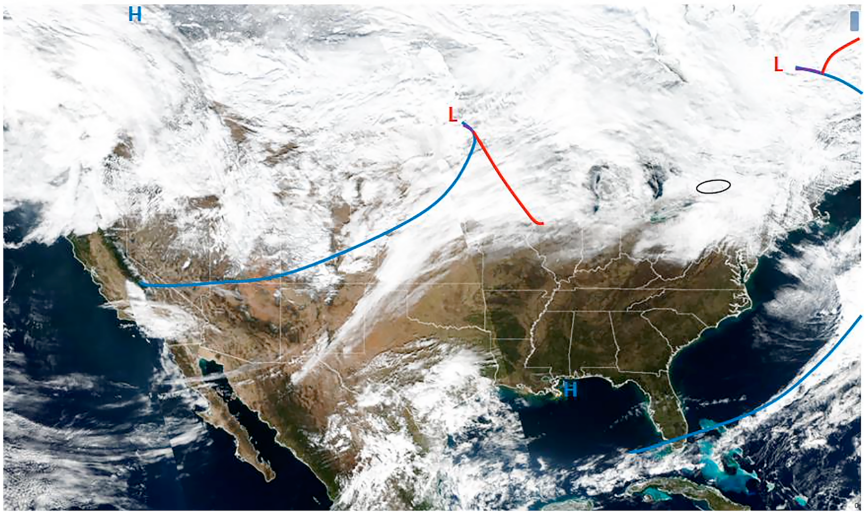

FIG. 14. Synoptic conditions observed on 1200 UTC 12 Jan 2014 [Daily Weather Maps (https://www.wpc.ncep.noaa.gov/dailywxmap/index_20140112.html), accessed 23 Feb 2022].

nearby synoptic systems (cyclones, fronts) were visible in satellite imagery and appeared in regional soundings analyses, respectively (such as Figs. 14 and 16). Except for the LWC method, the remaining CBL detection criteria mentioned in this study performed poorly (Fig. 17) when tested using IOA and R metrics for decoupled boundary layer cases when compared with the coupled boundary layers. This poor performance could be due to the surface connected boundary layer not having proper mixed layer and a strong capping inversion as seen from Fig. 15, and/or the lack of many observed decoupled boundary layers in the present dataset. The potential for EMLs to increase lake-effect snowfall rates above that expected for coupled CBLs suggests that further study is needed to fully understand their evolution.

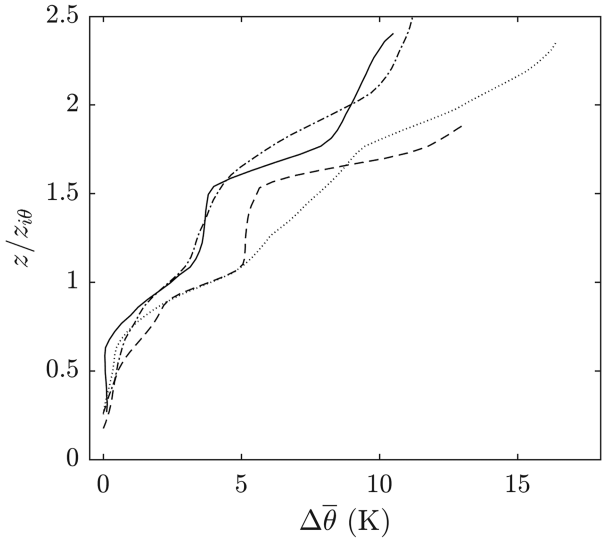

FIG. 15. As in Fig. 12a, but for LE PBL cases with elevated mixed layers.

After studying the different lake-effect boundary layer structures in the present database (e.g., well-mixed, not well-mixed, multiple cloud layers, coupled, and elevated mixed layers), we would like to point out that similar modification of cold air moving over warm water can be observed for wintertime cold-air outbreaks (CAOs) especially in the high latitudes (Wayland and Raman 1989; Brümmer et al. 1992; Brümmer 1996; Hartmann et al. 1997). Similar to downwind boundary layer deepening along the lake during lake effects, the boundary layer deepens with fetch during cold-air outbreaks as well (Wayland and Raman 1989; Wu and Ovchinnikov 2022; Michaelis et al. 2022). Another similarity between the cold-air outbreaks and the lake-effect systems is the presence of cloud layering within the boundary layer. Recently, using the observations collected from December 2019 to May 2020 during the CAOs in the Marine Boundary Layer Experiment (COMBLE; Geerts et al. 2022), Lackner et al. (2023) studied the vertical structure of the clouds formed due to Arctic air mass advected over warm water and found that single cloud layers occurred for only about 60% of the time, while two or more cloud layers are observed for 35% of the time during the CAOs over Arctic. To the authors knowledge, a systematic study of evaluating the performance of CBL depth estimation methods in boundary layers modified by cold-air outbreaks is not performed yet and such an analysis would be beneficial to test the outcomes presented in this study, especially the sensitivity of the methods when there are multiple cloud layers present.

6. Summary

Research aircraft observations conducting flights conducive for atmospheric sounding development during OWLeS, and Lake-ICE field campaigns were used to obtain the CBL depth by different methods. The CBL depth estimated by the turbulence method was considered to be the reference value and was compared with the CBL depth estimated by gradient

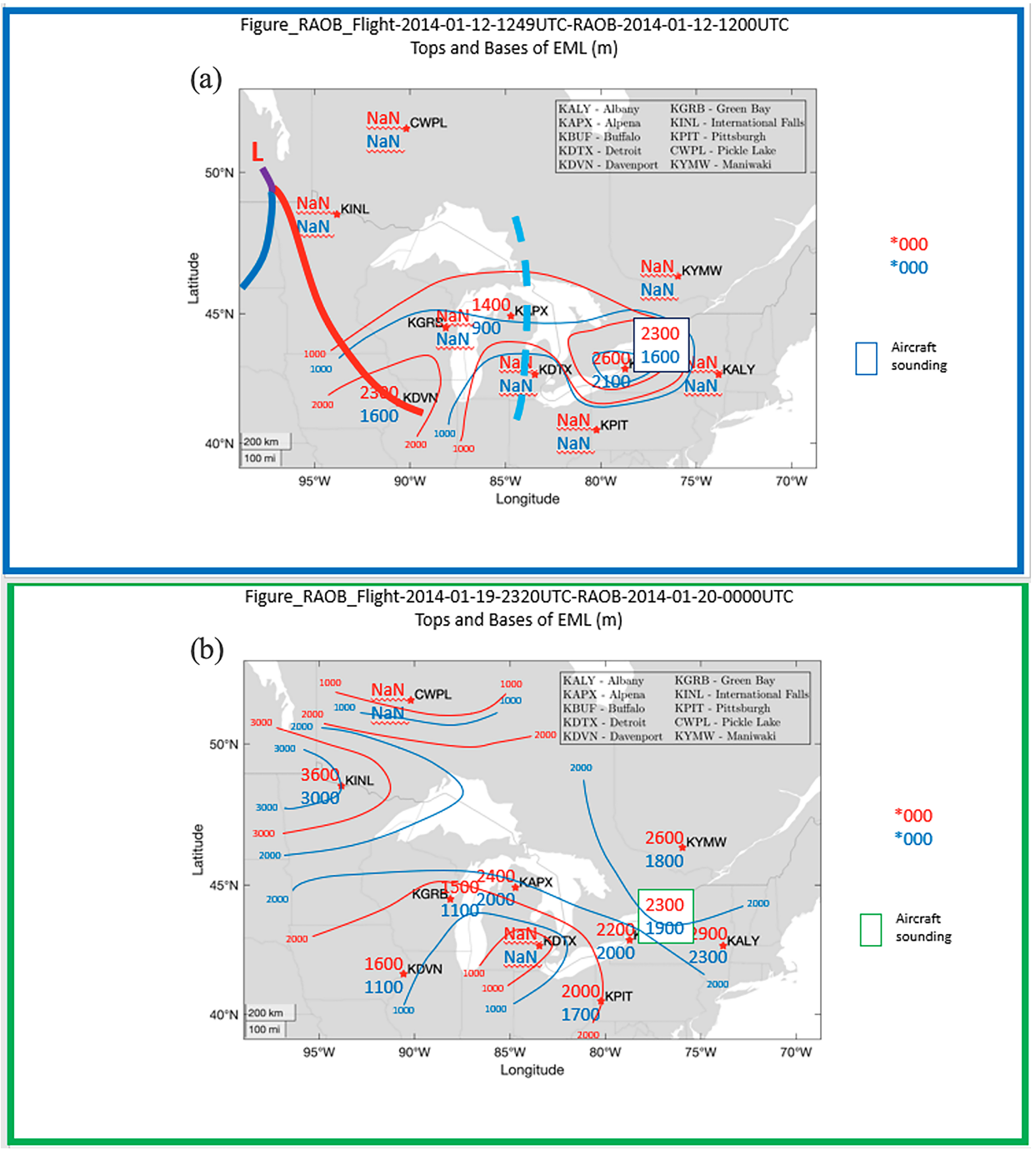

FIG. 16. EML top (red) and base (blue) observed from NOAA sounding data from stations (plotted as red stars) located around the Great Lakes region on (a) 1200 UTC 12 Jan 2014and (b) 0000 UTC 19 Jan 2014. "NaN" indicates that no EMLs were identified. The aircraft sounding location and EML depths extracted are given in the white boxes.

methods of potential temperature, relative humidity, mixing ratio, bulk Richardson number method, and liquid water content method for soundings that went through clouds. Each method's performance was calculated using the mean errors (MAE and MBE), centered RMSE and IOA metrics. The potential temperature gradient method performed well for soundings over lake and land, while the bulk Richardson number method performed poorly and consistently underestimating the CBL depth. We tested the performance of methods by averaging the aircraft observations using different vertical averaging windows ranging from 5 to 300 m. The effect of vertical averaging depth was more prominent on the

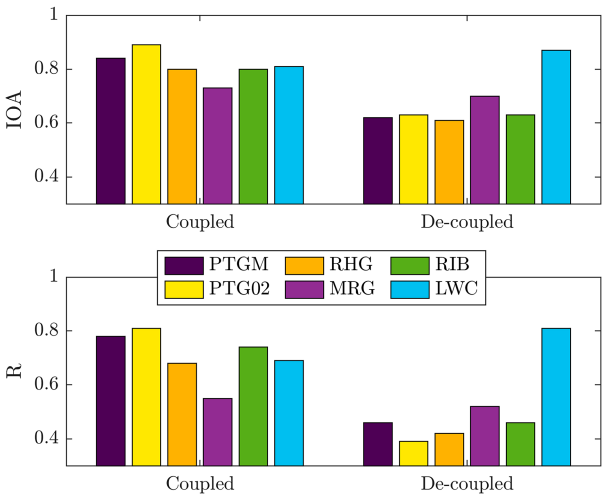

FIG. 17. Comparison of (top) IOA and (bottom) *R* between coupled and decoupled boundary layers observed during OWLeS and Lake-ICE.

temperature gradient and bulk Richardson number methods. For all the methods tested, 20- and 50-m vertical averaging resulted in similar performance. We also tested the sensitivity of the threshold value for the potential temperature gradient method and our results suggest using 0.015 and 0.011 K m^{-1} for soundings that are averaged using 50-m vertical window over land and lake, respectively. These threshold values were seen to increase with decreases in vertical averaging window depth. Using potential temperature profile, the maximum gradient method also gave good results with IOA of 0.76 after the gradient threshold value method whose IOA was 0.81. Thus, we recommend using the potential temperature gradient method (either threshold based, or maximum gradient based) for estimating the CBL depth during LE conditions. For cloud-topped boundary layers, the liquid water content method gave good performance similar to the potential temperature gradient method.

For a given percentage allowable error, the efficiency of methods tested was variable for soundings taken over lake, while it is similar for soundings taken over land. We hypothesize that the lake surface being warmer than the air over it adds energy into the boundary layer making it active leading to subtle differences in the thermodynamic profiles. Lack of radiosonde observations over the lake makes it difficult to further analyze these differences. We note that LE boundary layers could be coupled with a well-defined mixed layer topped with an inversion or decoupled with multiple mixed layers and inversions. Such decoupled boundary layers identified in this dataset were accompanied by either a nearby front or a synoptic storm system. Given the potential large influences of elevated mixed layers on LE systems, further detailed study is warranted.

Acknowledgments. Funding for this study was provided from National Science Foundation (NSF) Award AGS 20-15672. Opinions expressed are those of the authors and not necessarily those of the Illinois State Water Survey, the Prairie Research Institute, the University of Illinois, or the NSF. The authors declare that there is no conflict of interest.

Data availability statement. All the data used in this study are openly available from EOL database for Lake-ICE (https://doi.org/10.26023/5VWZ-PGAN-PC0E) and UWKA database for OWLeS (http://flights.uwyo.edu/projects/owles13/order_25hz.shtml).

REFERENCES

Agee, E. M., and S. R. Gilbert, 1989: An aircraft investigation of mesoscale convection over Lake Michigan during the 10 January 1984 cold air outbreak. *J. Atmos. Sci.*, **46**, 1877–1897, https://doi.org/10.1175/1520-0469(1989)046<1877:AAIOMC>2.0.CO;2.

——, and M. L. Hart, 1990: Boundary layer and mesoscale structure over Lake Michigan during a wintertime cold air outbreak. *J. Atmos. Sci.*, **47**, 2293–2316, https://doi.org/10.1175/1520-0469(1990)047<2293:BLAMSO>2.0.CO;2.

Ao, C. O., T. K. Chan, B. A. Iijima, J. L. Li, A. J. Mannucci, J. Teixeira, B. Tian, and D. E. Waliser, 2008: Planetary boundary layer information from GPS radio occultation measurements. *GRAS SAF Workshop on Applications of GPSRO Measurements*, Reading, United Kingdom, ECMWF and EUMETSAT, 123–131, https://www.ecmwf.int/en/elibrary/73224-planetary-boundary-layer-information-gps-radio-occultation-measurements.

Barthold, F. E., and D. A. R. Kristovich, 2011: Observations of the cross-lake cloud and snow evolution in a lake-effect snow event. *Mon. Wea. Rev.*, **139**, 2386–2398, https://doi.org/10.1175/MWR-D-10-05001.1.

Bergmaier, P. T., and B. Geerts, 2020: LLAP band structure and intense lake-effect snowfall downwind of Lake Ontario: Insights from the OWLeS 7–9 January 2014 event. *J. Appl. Meteor. Climatol.*, **59**, 1691–1715, https://doi.org/10.1175/JAMC-D-19-0288.1.

——, ——, L. S. Campbell, and W. J. Steenburgh, 2017: The OWLeS IOP2b lake-effect snowstorm: Dynamics of the secondary circulation. *Mon. Wea. Rev.*, **145**, 2437–2459, https://doi.org/10.1175/MWR-D-16-0462.1.

Bianco, L., and J. M. Wilczak, 2002: Convective boundary layer depth: Improved measurement by Doppler radar wind profiler using fuzzy logic methods. *J. Atmos. Oceanic Technol.*, **19**, 1745–1758, https://doi.org/10.1175/1520-0426(2002)019<1745:CBLDIM>2.0.CO;2.

Braham, R. R., Jr., and M. J. Dungey, 1995: Lake-effect snowfall over Lake Michigan. *J. Appl. Meteor.*, **34**, 1009–1019, https://doi.org/10.1175/1520-0450(1995)034<1009:LESOLM>2.0.CO;2.

Bretherton, C. S., and M. C. Wyant, 1997: Moisture transport, lower-tropospheric stability, and decoupling of cloud-topped boundary layers. *J. Atmos. Sci.*, **54**, 148–167, https://doi.org/10.1175/1520-0469(1997)054<0148:MTLTSA>2.0.CO;2.

Brümmer, B., 1996: Boundary-layer modification in wintertime cold-air outbreaks from the Arctic sea ice. *Bound.-Layer Meteor.*, **80**, 109–125, https://doi.org/10.1007/BF00119014.

——, B. Rump, and G. Kruspe, 1992: A cold air outbreak near Spitsbergen in springtime—Boundary-layer modification and cloud development. *Bound.-Layer Meteor.*, **61**, 13–46, https://doi.org/10.1007/BF02033993.

Campbell, L. S., and W. J. Steenburgh, 2017: The OWLeS IOP2b lake-effect snowstorm: Mechanisms contributing to the Tug

Hill precipitation maximum. *Mon. Wea. Rev.*, **145**, 2461–2478, https://doi.org/10.1175/MWR-D-16-0461.1.

——, ——, P. G. Veals, T. W. Letcher, and J. R. Minder, 2016: Lake-effect mode and precipitation enhancement over the Tug Hill Plateau during OWLeS IOP2b. *Mon. Wea. Rev.*, **144**, 1729–1748, https://doi.org/10.1175/MWR-D-15-0412.1.

Chang, J. C., and S. R. Hanna, 2004: Air quality model performance evaluation. *Meteor. Atmos. Phys.*, **87**, 167–196, https://doi.org/10.1007/s00703-003-0070-7.

Chang, S. S., and R. R. Braham Jr., 1991: Observational study of a convective internal boundary layer over Lake Michigan. *J. Atmos. Sci.*, **48**, 2265–2279, https://doi.org/10.1175/1520-0469(1991)048<2265:OSOACI>2.0.CO;2.

Chen, X., T. Yang, Z. Wang, F. Wang, and H. Wang, 2023: An ensemble method for improving the estimation of planetary boundary layer height from radiosonde data. *Atmos. Meas. Tech.*, **16**, 4289–4302, https://doi.org/10.5194/amt-16-4289-2023.

Cooper, K. A., M. R. Hjelmfelt, R. G. Derickson, D. A. R. Kristovich, and N. F. Laird, 2000: Numerical simulation of transitions in boundary layer convective structures in a lake-effect snow event. *Mon. Wea. Rev.*, **128**, 3283–3295, https://doi.org/10.1175/1520-0493(2000)128<3283:NSOTIB>2.0.CO;2.

Dai, C., Z. Gao, Q. Wang, and G. Cheng, 2011: Analysis of atmospheric boundary layer height characteristics over the Arctic Ocean using the aircraft and GPS soundings. *Atmos. Ocean. Sci. Lett.*, **4**, 124–130, https://doi.org/10.1080/16742834.2011.11446916.

——, Q. Wang, J. A. Kalogiros, D. H. Lenschow, Z. Gao, and M. Zhou, 2014: Determining boundary-layer height from aircraft measurements. *Bound.-Layer Meteor.*, **152**, 277–302, https://doi.org/10.1007/s10546-014-9929-z.

Dong, X., B. Xi, and P. Wu, 2014: Investigation of the diurnal variation of marine boundary layer cloud microphysical properties at the Azores. *J. Climate*, **27**, 8827–8835, https://doi.org/10.1175/JCLI-D-14-00434.1.

Duncan, J. B., Jr., and Coauthors, 2022: Evaluating convective planetary boundary layer height estimations resolved by both active and passive remote sensing instruments during the CHEESEHEAD19 field campaign. *Atmos. Meas. Tech.*, **15**, 2479–2502, https://doi.org/10.5194/amt-15-2479-2022.

Eipper, D. T., G. S. Young, S. J. Greybush, S. Saslo, T. D. Sikora, and R. D. Clark, 2018: Predicting the inland penetration of long-lake-axis-parallel snowbands. *Wea. Forecasting*, **33**, 1435–1451, https://doi.org/10.1175/WAF-D-18-0033.1.

——, S. J. Greybush, G. S. Young, S. Saslo, T. D. Sikora, and R. D. Clark, 2019: Lake-effect snowbands in baroclinic environments. *Wea. Forecasting*, **34**, 1657–1674, https://doi.org/10.1175/WAF-D-18-0191.1.

Garc, J. A., M. L. Cancillo, and J. L. Cano, 2002: A case study of the morning evolution of the convective boundary layer depth. *J. Appl. Meteor.*, **41**, 1053–1059, https://doi.org/10.1175/1520-0450(2002)041<1053:ACSOTM>2.0.CO;2.

Garratt, J. R., 1994: Review: The atmospheric boundary layer. *Earth-Sci. Rev.*, **37**, 89–134, https://doi.org/10.1016/0012-8252(94)90026-4.

Geerts, B., and Coauthors, 2022: The COMBLE campaign: A study of marine boundary layer clouds in Arctic cold-air outbreaks. *Bull. Amer. Meteor. Soc.*, **103**, E1371–E1389, https://doi.org/10.1175/BAMS-D-21-0044.1.

Ghate, V. P., M. A. Miller, B. A. Albrecht, and C. W. Fairall, 2015: Thermodynamic and radiative structure of stratocumulus-topped boundary layers. *J. Atmos. Sci.*, **72**, 430–451, https://doi.org/10.1175/JAS-D-13-0313.1.

Greybush, S. J., G. S. Young, T. D. Sikora, S. Saslo, R. D. Clark, and M. L. Jurewicz, 2018: Formation and evolution of elevated mixed layers in the Great Lakes lake-effect environment. *22nd Conf. on Integrated Observing and Assimilation Systems for the Atmosphere, Oceans, and Land Surface*, Austin, TX, Amer. Meteor. Soc., 1049, https://ams.confex.com/ams/98Annual/meetingapp.cgi/Paper/331330.

Grimsdell, A. W., and W. M. Angevine, 1998: Convective boundary layer height measurement with wind profilers and comparison to cloud base. *J. Atmos. Oceanic Technol.*, **15**, 1331–1338, https://doi.org/10.1175/1520-0426(1998)015<1331:CBLHMW>2.0.CO;2.

Guo, J., and Coauthors, 2021: Investigation of near-global daytime boundary layer height using high-resolution radiosondes: First results and comparison with ERA5, MERRA-2, JRA-55, and NCEP-2 reanalyses. *Atmos. Chem. Phys.*, **21**, 17 079–17 097, https://doi.org/10.5194/acp-21-17079-2021.

Hartmann, J., C. Kottmeier, and S. Raasch, 1997: Roll vortices and boundary-layer development during a cold air outbreak. *Bound.-Layer Meteor.*, **84**, 45–65, https://doi.org/10.1023/A:1000392931768.

Hennemuth, B., and A. Lammert, 2006: Determination of the atmospheric boundary layer height from radiosonde and lidar backscatter. *Bound.-Layer Meteor.*, **120**, 181–200, https://doi.org/10.1007/s10546-005-9035-3.

Hong, S.-Y., Y. Noh, and J. Dudhia, 2006: A new vertical diffusion package with an explicit treatment of entrainment processes. *Mon. Wea. Rev.*, **134**, 2318–2341, https://doi.org/10.1175/MWR3199.1.

Jones, C. R., C. S. Bretherton, and D. Leon, 2011: Coupled vs. decoupled boundary layers in VOCALS-REx. *Atmos. Chem. Phys.*, **11**, 7143–7153, https://doi.org/10.5194/acp-11-7143-2011.

Jozef, G., J. Cassano, S. Dahlke, and G. de Boer, 2022: Testing the efficacy of atmospheric boundary layer height detection algorithms using uncrewed aircraft system data from MOSAiC. *Atmos. Meas. Tech.*, **15**, 4001–4022, https://doi.org/10.5194/amt-15-4001-2022.

Kaimal, J. C., and Coauthors, 1982: Estimating the depth of the daytime convective boundary layer. *J. Appl. Meteor.*, **21**, 1123–1129, https://doi.org/10.1175/1520-0450(1982)021<1123:ETDOTD>2.0.CO;2.

Kosiba, K. A., J. Wurman, K. Knupp, K. Pennington, and P. Robinson, 2019: Ontario Winter Lake-effect Systems (OWLeS): Bulk characteristics and kinematic evolution of misovortices in long-lake-axis-parallel snowbands. *Mon. Wea. Rev.*, **148**, 131–157, https://doi.org/10.1175/MWR-D-19-0182.1.

Kotthaus, S., and Coauthors, 2023: Atmospheric boundary layer height from ground-based remote sensing: A review of capabilities and limitations. *Atmos. Meas. Tech.*, **16**, 433–479, https://doi.org/10.5194/amt-16-433-2023.

Kristovich, D. A. R., and R. R. Braham Jr., 1998: Mean profiles of moisture fluxes in snow-filled boundary layers. *Bound.-Layer Meteor.*, **87**, 195–215, https://doi.org/10.1023/A:1000836401204.

——, and Coauthors, 2000: The Lake-Induced Convection Experiment and the Snowband Dynamics Project. *Bull. Amer. Meteor. Soc.*, **81**, 519–542, https://doi.org/10.1175/1520-0477(2000)081<0519:TLCEAT>2.3.CO;2.

——, N. F. Laird, and M. R. Hjelmfelt, 2003: Convective evolution across Lake Michigan during a widespread lake-effect snow event. *Mon. Wea. Rev.*, **131**, 643–655, https://doi.org/10.1175/1520-0493(2003)131<0643:CEALMD>2.0.CO;2.

——, and Coauthors, 2017: The Ontario Winter Lake-Effect Systems field campaign: Scientific and educational adventures to further our knowledge and prediction of lake-effect storms. *Bull. Amer. Meteor. Soc.*, **98**, 315–332, https://doi.org/10.1175/BAMS-D-15-00034.1.

——, L. Bard, L. Stoecker, and B. Geerts, 2018: Influence of Lake Erie on a Lake Ontario lake-effect snowstorm. *J. Appl. Meteor. Climatol.*, **57**, 2019–2033, https://doi.org/10.1175/JAMC-D-17-0349.1.

——, E. Takle, G. S. Young, and A. Sharma, 2019: 100 years of progress in mesoscale planetary boundary layer meteorological research. *A Century of Progress in Atmospheric and Related Sciences: Celebrating the American Meteorological Society Centennial*, *Meteor. Monogr.*, No. 59, Amer. Meteor. Soc., https://doi.org/10.1175/AMSMONOGRAPHS-D-18-0023.1.

Lackner, C. P., B. Geerts, T. W. Juliano, L. Xue, and B. Kosovic, 2023: Vertical structure of clouds and precipitation during Arctic cold-air outbreaks and warm-air intrusions: Observations from COMBLE. *J. Geophys. Res. Atmos.*, **128**, e2022JD038403, https://doi.org/10.1029/2022JD038403.

Laird, N. F., and D. A. R. Kristovich, 2004: Comparison of observations with idealized model results for a method to resolve winter lake-effect mesoscale morphology. *Mon. Wea. Rev.*, **132**, 1093–1103, https://doi.org/10.1175/1520-0493(2004)132<1093:COOWIM>2.0.CO;2.

LeMone, M. A., M. Tewari, F. Chen, and J. Dudhia, 2013: Objectively determined fair-weather CBL depths in the ARW-WRF model and their comparison to CASES-97 observations. *Mon. Wea. Rev.*, **141**, 30–54, https://doi.org/10.1175/MWR-D-12-00106.1.

——, and Coauthors, 2019: 100 years of progress in boundary layer meteorology. *A Century of Progress in Atmospheric and Related Sciences: Celebrating the American Meteorological Society Centennial*, *Meteor. Monogr.*, No. 59, Amer. Meteor. Soc., https://doi.org/10.1175/AMSMONOGRAPHS-D-18-0013.1.

Lenschow, D. H., 1973: Two examples of planetary boundary layer modification over the Great Lakes. *J. Atmos. Sci.*, **30**, 568–581, https://doi.org/10.1175/1520-0469(1973)030<0568:TEOPBL>2.0.CO;2.

——, M. Zhou, X. Zeng, L. Chen, and X. Xu, 2000: Measurements of fine-scale structure at the top of marine stratocumulus. *Bound.-Layer Meteor.*, **97**, 331–357, https://doi.org/10.1023/A:1002780019748.

Li, H., B. Liu, X. Ma, S. Jin, Y. Ma, Y. Zhao, and W. Gong, 2021: Evaluation of retrieval methods for planetary boundary layer height based on radiosonde data. *Atmos. Meas. Tech.*, **14**, 5977–5986, https://doi.org/10.5194/amt-14-5977-2021.

Martucci, G., R. Matthey, V. Mitev, and H. Richner, 2007: Lidar determination of the frequency of variations of the boundary-layer top. *Proc. 2007 IEEE Int. Geoscience and Remote Sensing Symp.*, Barcelona, Spain, Institute of Electrical and Electronics Engineers, 2767–2770, https://doi.org/10.1109/IGARSS.2007.4423416.

Michaelis, J., A. U. Schmitt, C. Lüpkes, J. Hartmann, G. Birnbaum, and T. Vihma, 2022: Observations of marine cold-air outbreaks: A comprehensive data set of airborne and dropsonde measurements from the Springtime Atmospheric Boundary Layer Experiment (STABLE). *Earth Syst. Sci. Data*, **14**, 1621–1637, https://doi.org/10.5194/essd-14-1621-2022.

Minder, J. R., T. W. Letcher, L. S. Campbell, P. G. Veals, and W. J. Steenburgh, 2015: The evolution of lake-effect convection during landfall and orographic uplift as observed by profiling radars. *Mon. Wea. Rev.*, **143**, 4422–4442, https://doi.org/10.1175/MWR-D-15-0117.1.

Moeng, C.-H., B. Stevens, and P. P. Sullivan, 2005: Where is the interface of the stratocumulus-topped PBL? *J. Atmos. Sci.*, **62**, 2626–2631, https://doi.org/10.1175/JAS3470.1.

Mulholland, J. P., J. Frame, S. W. Nesbitt, S. M. Steiger, K. A. Kosiba, and J. Wurman, 2017: Observations of misovortices within a long-lake-axis-parallel lake-effect snowband during the OWLeS project. *Mon. Wea. Rev.*, **145**, 3265–3291, https://doi.org/10.1175/MWR-D-16-0430.1.

Niziol, T. A., 1987: Operational forecasting of lake effect snowfall in western and central New York. *Wea. Forecasting*, **2**, 310–321, https://doi.org/10.1175/1520-0434(1987)002<0310:OFOLES>2.0.CO;2.

——, W. R. Snyder, and J. S. Waldstreicher, 1995: Winter weather forecasting throughout the eastern United States. Part IV: Lake effect snow. *Wea. Forecasting*, **10**, 61–77, https://doi.org/10.1175/1520-0434(1995)010<0061:WWFTTE>2.0.CO;2.

Nowak, J. L., H. Siebert, K. E. Szodry, and S. P. Malinowski, 2021: Coupled and decoupled stratocumulus-topped boundary layers: Turbulence properties. *Atmos. Chem. Phys.*, **21**, 10 965–10 991, https://doi.org/10.5194/acp-21-10965-2021.

Pleim, J. E., 2007: A combined local and nonlocal closure model for the atmospheric boundary layer. Part I: Model description and testing. *J. Appl. Meteor. Climatol.*, **46**, 1383–1395, https://doi.org/10.1175/JAM2539.1.

Rodriguez, R., D. A. R. Kristovich, and M. R. Hjelmfelt, 2007: Lake-to-lake cloud bands: Frequencies and locations. *Mon. Wea. Rev.*, **135**, 4202–4213, https://doi.org/10.1175/2007MWR1960.1.

Sagrestano, S. M., 2023: Use of airborne lidar for boundary layer entrainment zone observations. M.S. thesis, Dept. of Atmospheric Sciences, University of Illinois, 65 pp.

Santanello, J. A., Jr., M. A. Friedl, and W. P. Kustas, 2005: An empirical investigation of convective planetary boundary layer evolution and its relationship with the land surface. *J. Appl. Meteor.*, **44**, 917–932, https://doi.org/10.1175/JAM2240.1.

Schroeder, J. J., D. A. R. Kristovich, and M. R. Hjelmfelt, 2006: Boundary layer and microphysical influences of natural cloud seeding on a lake-effect snowstorm. *Mon. Wea. Rev.*, **134**, 1842–1858, https://doi.org/10.1175/MWR3151.1.

Seibert, P., F. Beyrich, S.-E. Gryning, S. Joffre, A. Rasmussen, and P. Tercier, 2000: Review and intercomparison of operational methods for the determination of the mixing height. *Atmos. Environ.*, **34**, 1001–1027, https://doi.org/10.1016/S1352-2310(99)00349-0.

Seidel, D. J., C. O. Ao, and K. Li, 2010: Estimating climatological planetary boundary layer heights from radiosonde observations: Comparison of methods and uncertainty analysis. *J. Geophys. Res.*, **115**, D16113, https://doi.org/10.1029/2009JD013680.

——, Y. Zhang, A. Beljaars, J.-C. Golaz, A. R. Jacobson, and B. Medeiros, 2012: Climatology of the planetary boundary layer over the continental United States and Europe. *J. Geophys. Res.*, **117**, D17106, https://doi.org/10.1029/2012JD018143.

Steenburgh, W. J., and L. S. Campbell, 2017: The OWLeS IOP2b lake-effect snowstorm: Shoreline geometry and the mesoscale forcing of precipitation. *Mon. Wea. Rev.*, **145**, 2421–2436, https://doi.org/10.1175/MWR-D-16-0460.1.

Steiger, S. M., T. Kranz, and T. W. Letcher, 2018: Thunderstorm characteristics during the Ontario Winter Lake-Effect

Systems project. *J. Appl. Meteor. Climatol.*, **57**, 853–874, https://doi.org/10.1175/JAMC-D-17-0188.1.

Stull, R. B., 1988: *An Introduction to Boundary Layer Meteorology*. Vol. 13. Springer Science & Business Media, 670 pp.

Su, T., Y. Zheng, and Z. Li, 2022: Methodology to determine the coupling of continental clouds with surface and boundary layer height under cloudy conditions from Lidar and meteorological data. *Atmos. Chem. Phys.*, **22**, 1453–1466, https://doi.org/10.5194/acp-22-1453-2022.

Veals, P. G., W. J. Steenburgh, and L. S. Campbell, 2018: Factors affecting the inland and orographic enhancement of lake-effect precipitation over the Tug Hill Plateau. *Mon. Wea. Rev.*, **146**, 1745–1762, https://doi.org/10.1175/MWR-D-17-0385.1.

Vogelezang, D. H. P., and A. A. M. Holtslag, 1996: Evaluation and model impacts of alternative boundary-layer height formulations. *Bound.-Layer Meteor.*, **81**, 245–269, https://doi.org/10.1007/BF02430331.

Wang, Q., and S. Wang, 2004: Turbulent and thermodynamic structure of the autumnal Arctic boundary layer due to embedded clouds. *Bound.-Layer Meteor.*, **113**, 225–247, https://doi.org/10.1023/B:BOUN.0000039375.41823.22.

——, and Coauthors, 1999: Characteristics of the marine boundary layers during two Lagrangian measurement periods: 2. Turbulence structure. *J. Geophys. Res.*, **104**, 21 767–21 784, https://doi.org/10.1029/1998JD100100.

Wang, X. Y., and K. C. Wang, 2014: Estimation of atmospheric mixing layer height from radiosonde data. *Atmos. Meas. Tech.*, **7**, 1701–1709, https://doi.org/10.5194/amt-7-1701-2014.

Wayland, R. J., and S. Raman, 1989: Mean and turbulent structure of a baroclinic marine boundary layer during the 28 January 1986 cold-air outbreak (GALE 86). *Bound.-Layer Meteor.*, **48**, 227–254, https://doi.org/10.1007/BF00158326.

Welsh, D., B. Geerts, X. Jing, P. T. Bergmaier, J. R. Minder, W. J. Steenburgh, and L. S. Campbell, 2016: Understanding heavy lake-effect snowfall: The vertical structure of radar reflectivity in a deep snowband over and downwind of Lake Ontario. *Mon. Wea. Rev.*, **144**, 4221–4244, https://doi.org/10.1175/MWR-D-16-0057.1.

Wood, R., and C. S. Bretherton, 2004: Boundary layer depth, entrainment, and decoupling in the cloud-capped subtropical and tropical marine boundary layer. *J. Climate*, **17**, 3576–3588, https://doi.org/10.1175/1520-0442(2004)017<3576:BLDEAD>2.0.CO;2.

Wu, P., and M. Ovchinnikov, 2022: Cloud morphology evolution in Arctic cold-air outbreak: Two cases during COMBLE period. *J. Geophys. Res. Atmos.*, **127**, e2021JD035966, https://doi.org/10.1029/2021JD035966.

Young, G. S., B. K. Cameron, and E. E. Hebble, 2000: Observations of the entrainment zone in a rapidly entraining boundary layer. *J. Atmos. Sci.*, **57**, 3145–3160, https://doi.org/10.1175/1520-0469(2000)057<3145:OOTEZI>2.0.CO;2.

Zeng, X., M. A. Brunke, M. Zhou, C. Fairall, N. A. Bond, and D. H. Lenschow, 2004: Marine atmospheric boundary layer height over the eastern Pacific: Data analysis and model evaluation. *J. Climate*, **17**, 4159–4170, https://doi.org/10.1175/JCLI3190.1.

Zhang, D., J. Comstock, and V. Morris, 2022: Comparison of planetary boundary layer height from ceilometer with ARM radiosonde data. *Atmos. Meas. Tech.*, **15**, 4735–4749, https://doi.org/10.5194/amt-15-4735-2022.

Zhang, J., and Coauthors, 2022: A climatology of merged daytime planetary boundary layer height over China from radiosonde measurements. *J. Geophys. Res. Atmos.*, **127**, e2021JD036367, https://doi.org/10.1029/2021JD036367.

Zhang, J. A., R. F. Rogers, D. S. Nolan, and F. D. Marks Jr., 2011: On the characteristic height scales of the hurricane boundary layer. *Mon. Wea. Rev.*, **139**, 2523–2535, https://doi.org/10.1175/MWR-D-10-05017.1.

Zhang, Y., Z. Gao, D. Li, Y. Li, N. Zhang, X. Zhao, and J. Chen, 2014: On the computation of planetary boundary-layer height using the bulk Richardson number method. *Geosci. Model Dev.*, **7**, 2599–2611, https://doi.org/10.5194/gmd-7-2599-2014.

Zurn-Birkhimer, S. M., E. M. Agee, and Z. Sorbjan, 2005: Convective structures in a cold air outbreak over Lake Michigan during Lake-ICE. *J. Atmos. Sci.*, **62**, 2414–2432, https://doi.org/10.1175/JAS3494.1.